DAS Departamento de Automação e Sistemas
CTC Centro Tecnológico
UFSC Universidade Federal de Santa Catarina

A cycle-power optimization strategy for airborne wind energy systems in pumping-kite mode

Report Submitted to the Federal University of Santa Catarina
as a requirement for approval in the course:
DAS 5511: Projeto de Fim de Curso

Lucas Napoleão Coelho

Florianópolis, December 2017

A cycle-power optimization strategy for airborne wind energy systems in pumping-kite mode

Lucas Napoleão Coelho

This work was evaluated in the context of the course:
DAS5511: Final Project Work
and was approved in its final form by the
Control and automation engineering undergraduate program

Julio Elias Normey-Rico

_____

Advisor's signature

Board of examiners:

Alexandre Trofino Neto
Supervisor

Julio Elias Normey-Rico
Academic advisor

Marcelo De Lellis Costa de Oliveira
Evaluator

Rhuan Carlos Boos
Debater

Vinícius David Woyakewicz
Debater

Agradecimentos

Ao professor Alexandre Trofino e aos demais integrantes do grupo UFSCKite, por possibilitarem o desenvolvimento deste trabalho em uma área desafiadora e relevante.

Ao professor Júlio Normey-Rico pela orientação ao longo do semestre e pelos amplos conhecimentos de controle passados. Também pela disponibilidade de diversas consultas ao longo do semestre e pela paciência e atenção apresentadas durante as mesmas.

Aos meus amigos e colegas de tabalho pelo apoio indispensável ao longo do semestre e pelas contribuições e sugstões prestadas ao longo de todo o desenvolvimento deste trabalho. Sem a convivência diária com estes, o documento aqui apresentado não seria possível.

Por fim, aos meus pais e familiares por tudo que estes me deram e cultivaram em mim ao longo da minha vida. Resultando finalmente no trabalho desenvolvido.

Resumo

Sistemas de geração baseados em aerofólios cabeados (AWES - Airborne Wind Energy Systems) correspondem a uma nova tecnologia para captação da energia eólica. No modo pumping-kite o aerofólio desenrola um cabo ligado a um tambor em solo, gerando energia através do desenrolamento do cabo sob alta tração. Após um período de geração, o cabo atinge um valor máximo e uma fase de recolhimento é iniciada. Nesta fase a máquina elétrica, antes utilizada como gerador, é acionada como motor gastando uma parcela da energia gerada para enrolar a quantia de cabo desenrolada. Para reduzir a energia gasta e prover um melhor aproveitamento ao sistema uma manobra de baixa tração do aerofólio é realizada durante o recolhimento do cabo.

A trajetória seguida pelo aerofólio, juntamente com a velocidade de desenrolamento e enrolamento do cabo e atuações adicionais que afetam o voo do aerofólio formam um conjunto complexo de variáveis que influenciam o saldo energético do sistema e, consequentemente, a viabilidade do mesmo. Devido à importância do tema, diversos trabalhos da literatura abordam esta tarefa, no entanto, uma solução definitiva ainda não foi encontrada.

Durante a fase de geração, é apresentada em [31] uma expressão para a velocidade de desenrolamento que maximiza a potência instantânea gerada. No entanto, uma potência média de ciclo mais elevada é obtida por uma velocidade de desenrolamento mais baixa, reduzindo a potência instantânea gerada e aumentando a duração da fase de geração. Este resultado é obtido em [12] através de uma otimização iterativa de todo o ciclo de operação. Neste mesmo trabalho é proposto um sistema de controle para manter o aerofólio em uma trajetória em lemniscata. Este trabalho adapta a otimização proposta em [12] para uma otimização on-line que determina a velocidade de desenrolamento e a elevação da trajetória em lemniscata ótimos. Ao operar com uma otimização on-line, consegue-se adaptar a solução para diferentes condições de vento e incorporar restrições físicas e de operação à solução encontrada.

Poucos trabalhos abordam em detalhes a geração de trajetória para a fase de recolhimento do aerofólio. Diversos trabalhos, como [14] e [17], abordam indiretamente este problema ao proporem um problema de otimização off-line para determinar uma trajetória completa de voo. Estes trabalhos, no entanto, fornecem uma solução para uma única condição de vento e empregam problemas de otimização muito complexos para serem executados em tempo real. Uma segunda abordagem utilizada é definir algumas características das referências utilizadas durante a fase de recolhimento. Em [23], por exemplo, o aerofólio é controlado através da tração e de uma atuação de

escoamento de vento, que modifica as propriedades aerodinâmicas do aerofólio e é comumente chamada de depower. Durante a fase de recolhimento, rampas de coeficientes fixos são utilizadas e o valor final de tração é determinado através de uma otimização iterativa ao longo de diversos ciclos de operação. Uma abordagem similar é utilizada para otimizar a fase de recolhimento em [12], que dá continuidade ao trabalho apresentado em [28]. Neste caso as referências de tração e depower também são limitadas a rampas, no entanto, as variáveis de decisão são os coeficientes das rampas.

Neste trabalho é proposto o emprego de um controle preditivo não-linear baseado em modelo (NMPC) com um critério econômico para aproximar a solução que otimiza a potência média de ciclo. Já é encontrado frequentemente na literatura o uso de NMPC para seguir trajetórias geradas off-line. Em contraste, neste trabalho propõe-se uma função custo que pondera a potência instantânea gasta e a velocidade de recolhimento a cada instante da trajetória. Esta função custo busca capturar o fator de decisão instantâneo que qualquer algoritmo de geração de trajetória deve realizar. A potência média de ciclo busca ser maximizada através de um breve estudo do efeito resultante da variação dos pesos da função custo. Os resultados obtidos mostram que a solução proposta atinge resultados similares à soluções off-line de otimização sendo suficientemente simples para ser executada on-line. O emprego de um NMPC permite a adição intuitiva de diversas restrições permitindo uma solução flexível e customizável.

A principal contribuição deste trabalho é o projeto de um algoritmo de otimização on-line para sistemas pumping-kite que apresenta bons resultados para diferentes condições de vento e possibilita a incorporação de diversas restrições de operação.

Palavras-chave: Energia eólica com aerofólios cabeados. Geração de trajetória. NMPC. Modo pumping-kite.

Abstract

Airborne wind energy systems (AWES) represent a novel high-altitude wind power harnessing technology in which the aerodynamic forces acting on suspended tethered aircraft are employed to produce electricity. In the so-called pumping-kite mode, the effects of such forces on the available aerodynamic surfaces are used to reel-out the tether and drive a generator on the ground, which is known as the traction phase. After a maximum tether length is reached the retraction phase takes place. During this part of the operating cycle, the tether is reeled back in while spending a fraction of the energy produced in the previous phase. In order to reduce the energy consumption and provide a better overall performance for the whole system, the trajectory of the aircraft must be carefully designed. This work proposes an on-line optimization strategy to adapt the airfoil trajectory to the current wind conditions and system parameters during both operation phases. The proposed algorithms, which were designed and tuned targeting an optimal average cycle-power, and also take into account the mutual influence of both phases of the pumping cycle, are shown to achieve performance levels similar to those obtained by more conventional off-line optimization methods while successfully complying with several operation and constructive constraints.

Key-words: Airborne wind energy. NMPC. Trajectory optimization. Pumping-kite mode.

Contents

List of Figures

List of Tables

Chapter 1

Introduction

The U.S Energy Information Administration (EIA) predicts that the global energy consumption will increase by 48% in the next 30 years. Given that production is still heavily dependent on fossil fuels – which are responsible for up to 86% of the total energy harvested directly from natural resources worldwide [4] – this dependency has the potential to severely impact the economy, similarly to what happened in 1970, when growth in consumption associated with political issues in the middle-east caused petroleum prices to spike overnight, leading to a generalized crisis [30]. Besides, studies show that the burn of substances such as petroleum derivatives and coal are likely the main culprits behind the severe climate and environmental changes that have been observed in the last few decades. Motivated by the many drawbacks associated with the consumption of fossil fuels, an increasing effort has been made by governments in order to leverage the use of renewable energy sources. The results of this effort can be seen in Figure 1.1, which depicts historical consumption trends for the most important energy sources, together with a prediction of their behavior for the upcoming years.

One of the most promising renewable energy sources is the wind. It is estimated that 13% of the world land area has winds faster than 6.9 m/s, which is more than enough to power the entire planet [6]. By 2015, wind power installed capacity was of approximately 432 GW, which is 22% more than that in 2014. According to the Global Wind Energy Council, wind energy accounted for 3.7% of the global electricity in that year.

After decades of enhancement, the conventional wind energy technology consists of a horizontal axis turbine mechanically coupled to three blades and mounted on the top of a tower. The evolution and scaling of this technology focuses on two main aspects: increases in the tower height, which results in having the blades exposed to stronger and more consistent winds, and increases in the turbine's diameter, so that a bigger area of wind can be intercepted. Although a continuous reduction of wind energy costs has been observed, most of the investment in wind farms still requires governmental subsidies or other kind of incentives in order to be economically attractive. A greater cost reduction is necessary to effectively change the scenario, yet, recent reports (e.g [5]) do not foresee any design changes in the near future capable of substantially reducing the cost of electricity produced by conventional wind turbines.

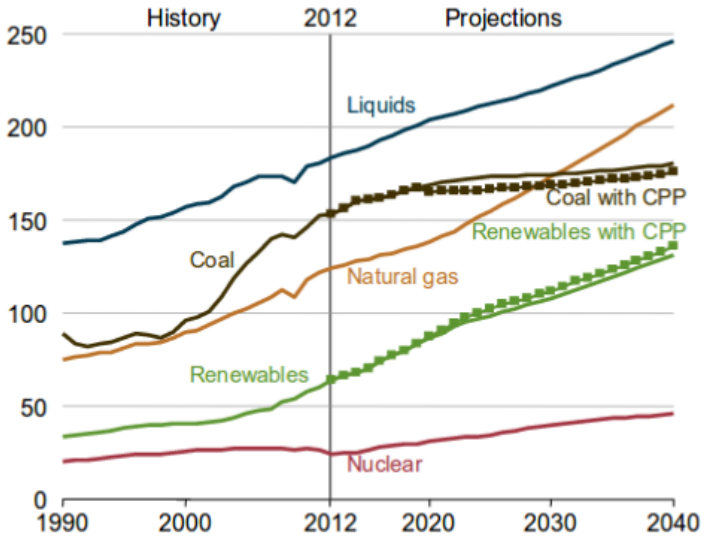

Figure 1.1: *Global energy consumption trend since 1990 together with a prediction for the next 30 years*

Source: [4]

This has motivated recent research for new technologies that can effectively lower this cost.

1.1 Airborne wind energy

Among the novel technologies for producing electricity from renewable resources, a new class of wind energy converters has been conceived under the name of Airborne Wind Energy (AWE) systems. This new generation of systems employs wings or aircraft in order to reach winds blowing at atmosphere layers that are inaccessible to traditional wind turbines [10]. AWE technology is able to reach higher altitudes than conventional wind turbines, where the wind is generally stronger and more consistent, as depicted in Figure 1.2, while allowing for a reduction in the construction and installation costs of the power plant. Moreover, since most locations offer a good wind potential at higher altitudes, deployment sites for AWE systems are much easier to find, which makes the technology even more appealing. These advantages do not come cheaply. The aircraft need to stay in constant movement to maintain themselves in the air, requiring a more complex control system. AWE systems replace an intrinsically stable system by an intrinsically unstable one [14].

AWE systems generally comprise two main components: a ground unit, and at least one aircraft that are mechanically or sometimes even electrically connected by

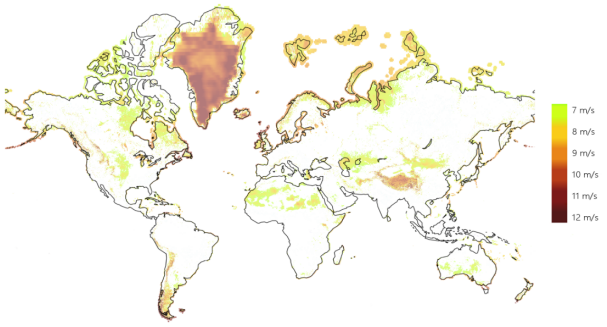

(a)

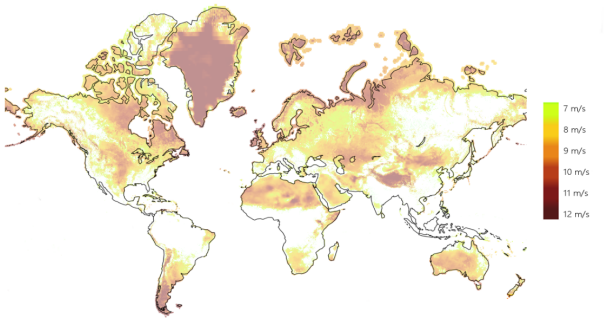

(b)

Figure 1.2: *Wind availability and average speed at (a) 50m; and (b) 200 m height. Darker colors identify regions with faster winds.*

Source: [29]

ropes, often referred to as tethers. Among the different concepts, one can distinguish ground-generation systems, in which the conversion of mechanical energy into electrical energy takes place on the ground, and airborne-generation systems, in which the conversion happens at the aircraft and the electricity is transferred to the ground through the tether.

In the last decade, developments in the AWE sector have experienced an extremely rapid acceleration. Several companies have entered the business of high-altitude wind energy, registering hundreds of patents and developing a number of prototypes and demonstrators. Research teams all over the world are currently working on different aspects of the technology, including control, electronics and mechanical design [10].

1.2 The UFSCkite group

The UFSCkite group was founded in late 2012 at the Department of Automation and Systems of the Federal University of Santa Catarina, in Florianópolis, Brazil. Its goal is to push the AWE technology forward towards the level of reliability, efficiency

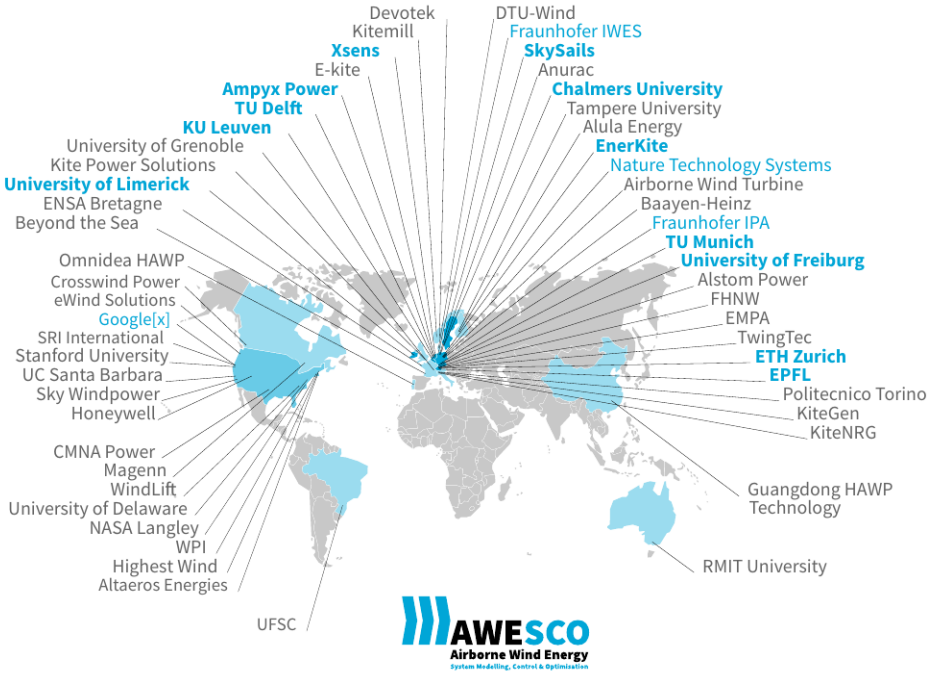

Figure 1.3: *The UFSCkite group as one of the institutions involved with AWE worldwide as of June 2015*

Source: [29]

and economical viability required for large-scale industrial deployment in the upcoming years. Starting with only three members, it has rapidly grown to a multidisciplinary team with expertise in areas such as modeling and simulation, filtering and flight control algorithms, industrial automation, power electronics, and embedded systems, carrying out research and development activities in a complementary fashion

The UFSCkite group is currently building a novel 12 kW ground-generation AWE prototype, which is expected to perform fully autonomous flight and produce electricity in order to demonstrate the concept of AWE to the academic community as well as to potential industry partners and investors.

1.3 Motivation

Despite the promising outlook in terms of economical feasibility, as pointed out in [11, 20], AWE technology is currently at an intermediate development stage, with several challenges yet to be overcome before it can reach the market. Tether technology, aerodynamics and wing design, sensors, control and energy conversion are all fields where AWE-oriented research is required either to solve technical bottlenecks or to improve off-the-shelf solutions that are being already used [16].

Ground-generation, or pumping-kite AWE systems with a fixed ground station such as that under development by the UFSCkite group represent the most common concept within the AWE community. The operation of these devices comprises a two-phase cycle. In the first phase, known as the traction, active, or generation phase, the aircraft is driven in a way to produce lift force, and consequently traction force on the tethers, which in turn induce the rotation of electrical generators. In the retraction, passive, or recovery phase, motors rewind the ropes thereby bringing the aircraft back to its original position with respect to the ground. In order to have a positive balance, the net energy produced in the generation phase has to be larger than the energy spent in the recovery phase. This positive balance must be guaranteed by the control systems, which are responsible for adjusting the aircraft's aerodynamic characteristics through the manipulation of control variables aiming at keeping it in flight and also at maximizing the cycle power.

The trajectory followed by the aircraft during the different phases of the pumping-cycle can vary, and has direct implication in the amount of power harvested from the wind, as it influences the magnitude of the lift force produced. While in the traction phase the most widely adopted approach is to fly in a circular or eight-shaped trajectory, in order to maximize the so called apparent wind and hence the traction force on the tether. On the other hand, the choice of an optimal trajectory for the retraction phase of pumping-kite systems still remains as one of the greatest challenges within AWE, given the sensitivity of the system to changes in the many inputs available, as well as to parameter uncertainty and wind disturbances.

1.4 Objectives

The aim of this work is to develop a cycle-power optimization strategy based on commonly available measurements and estimated variables for AWE systems operating in pumping-kite mode. The designed optimization scheme must yield, at every time instant of the digital control scheme, optimal values for variables such as the tether reeling speed and for the depower command, while allowing for stable operation during both the traction and retraction phases. Moreover, it must guarantee, to some extent, robustness in face of uncertainties and varying operating conditions such as wind gusts. Finally, all resulting algorithms must be validated in a simulation environment, and later adapted for integration into an actual AWE prototype.

More specifically, the purposes of this work are:

- To study cycle-power optimization approaches presented in the literature and already in use by the AWE community;

- To identify requirements, and to specify an optimization solution capable of meeting them;
- To design a solution according to the specifications resulting from the previous item, and to implement it in software;
- To evaluate the performance of the developed solution in a simulation environment, and determine its advantages and drawbacks with respect to other solutions in the literature.

1.5 Document structure

This document is organized as follows:

- Chapter 2 presents the AWE technology, trough a general overview, discussing the mathematical models used in this work and the UFSCkite system in detail, painting the full picture of where the developed solution will be applied;
- Chapter 3 provides a brief theoretical introduction to topics fundamental to the comprehension of the document, including an overview of Optimal Control Problems (OCP), and Nonlinear Model Predictive Control (NMPC) techniques. It also reviews the recent AWE literature, describing the current state-of-the-art in path optimization for pumping-kite systems;
- Chapter 4 presents the problems that motivated this work and fully states the proposed solution;
- Chapter 5 presents the implementation process of the solution, some problems found and the required changes and the results obtained in a simulation environment;
- Chapter 6 finally summarizes the accomplishments of this work, discusses its importance and limitations, and presents a series of subjects for future investigations.

1.6 Notation and units

Within this document vectors are denoted by bold characters, their Euclidean norm by $\|.\|$, and scalar values by non-bold characters. In situations involving more than one reference frame, the frame in which a vector is expressed is indicated by a superscript.

The symbol x_k indicates the k–th sample of a discrete signal x, and when the quantity represented by x is originally continuous, x_k refers to its discretized version. When charting vectorial signals, the x, y, and z components are represented in different colors, as indicated in the legend. Scalars are always charted in blue. Otherwise explicitly noted, all quantities are described in the International System of Units (SI).

Chapter 2

Airborne wind energy systems

Airborne Wind Energy (AWE) systems harvest wind power by exploiting the aerodynamic forces acting on lightweight suspended structures anchored to the ground by means of one or more tethers. This technology is able to reach higher altitudes than conventional wind turbines, where the wind is generally stronger and more consistent, while allowing for a reduction in the construction and installation costs of the power plant, among other advantages as discussed in [12, 11, 27, 24, 10].

Research on AWE systems started in the mid seventies, with a seminal work in [24], and despite the apparent abandonment during the nineties, the field recovered and experienced an extremely rapid expansion in the last decade. A number of systems based on different concepts have already been analyzed and tested.

Several institutions are entering the business of high-altitude wind energy, registering hundreds of patents and developing a number of prototypes and demonstrators. Research teams and companies all over the world are currently working on different aspects of the technology including control, electronics and mechanical design [10].

Currently, many companies have small-scale solutions that are not yet fully autonomous. These solutions are aimed to remote power and micro grids generation and generate around 30KW of power. This market already corresponds to an immense speculated market, however, the main accomplishment of such solutions was to validate the concept of AWE systems, attracting new investments for the next stage of the technology [19]. With a proven robust flight control and energy generation capabilities, investors now want to enable the existing solutions to scale up the generated power with some companies already planning to achieve 1MW of rated power by the end of the decade.

This chapter aims to provide a notion of what exists under the AWES umbrella and explain in detail the approach addressed in this work.

2.1 Classification

Apart from sharing the characteristic of using a structure suspended in the air to generate energy, the different approaches to AWE vary in several different aspects.

Due to the many differences in the existing approaches there are different classifications to AWES. The classifications hereafter presented are heavily based on [10].

According to this reference, AWES can be classified in terms of the principle that sustains the system in the air in two groups: systems that rely on aerostatic forces, and systems that depend on aerodynamic forces.

The systems based on aerostatic forces usually use gases lighter than the air, like helium, to float a generating structure connected to the ground through one or more tethers. The floating structure contains a generator, very similar to traditional wind turbines, adapted to work with higher wind speeds while having a low weight. Figure 2.1 shows a system based on this principle developed by the company Altaeros.

Figure 2.1: *Static aerogenerator constructed by Altaeros Energies [1].*

Systems that depend on aerodynamic forces for buoyancy can be further classified depending on the kind of aerodynamic force that they use to generate power. Since they depend on aerodynamic forces, all systems in this group need to stay in movement to stay airborne and are connected to the the ground by tethers for fixation and possibly to transfer generated energy. The first group exploits the drag forces in the systems trough mechanisms similar to traditional generators employed on-board. The second group exploits the lift force that is used to keep the systems in flight to traction a cable connected to a generator in the ground. In the latest approach it is necessary that the cable moves to generate power. This is achieved by either a moving generator or by a cable of variable length in combination to a reel-in back strategy.

(a) **(b)**

Figure 2.2: *AWES based in (b) drag forces and (a) lift forces.*

Source: Adapted from [2, 3]

Another common classification criterion is in terms of the generating unit location. Among the systems previously described, there are those that employ airborne generators that operate while flying, and some of them employ generators on the ground. The main implication of this difference is that systems that generate energy in flight are required to convert energy in the flying structure and transmit energy through the supporting cable. This results in more complex electrical subsystems and cable requirements. In ground generating systems this complexity resides in more traditional systems in the ground and the tethers that hold the airfoil only transmit mechanical energy to the generator. Systems representing each of these classes can be seen in figure 2.2

The final classification criterion presented here is in terms of the airfoil structure. This classification is fairly different for ground-generation and airborne-generation. Here will be presented only the classification for ground generation airfoil types since it is more relevant to this work.

Initially, a big number of research groups chose to use flexible airfoils since they can withstand fall damage and are usually cheaper than rigid or semi-rigid structures. However, these last are proven to have better aerodynamic efficiency and are easier to handle during landing and take-off procedures, making many companies choose to switch to these structures. Supporting Leading Edge (SLE) kites keep their form with inflated internal structures. This makes them easier to handle during landing and take-off in comparison to foil kites, that keep their form with the passing air. However, foil kites have higher aerodynamic efficiency, despite the higher number of bridles, and can be one order of magnitude larger in size.

Different airfoil structures depend on different control mechanisms, are subject to different physical limits and different wind forces. Therefore, to adapt the solutions proposed in this work to different airfoil structures it is necessary to adapt the mathematical

models, the control variables and the restrictions imposed in the model.

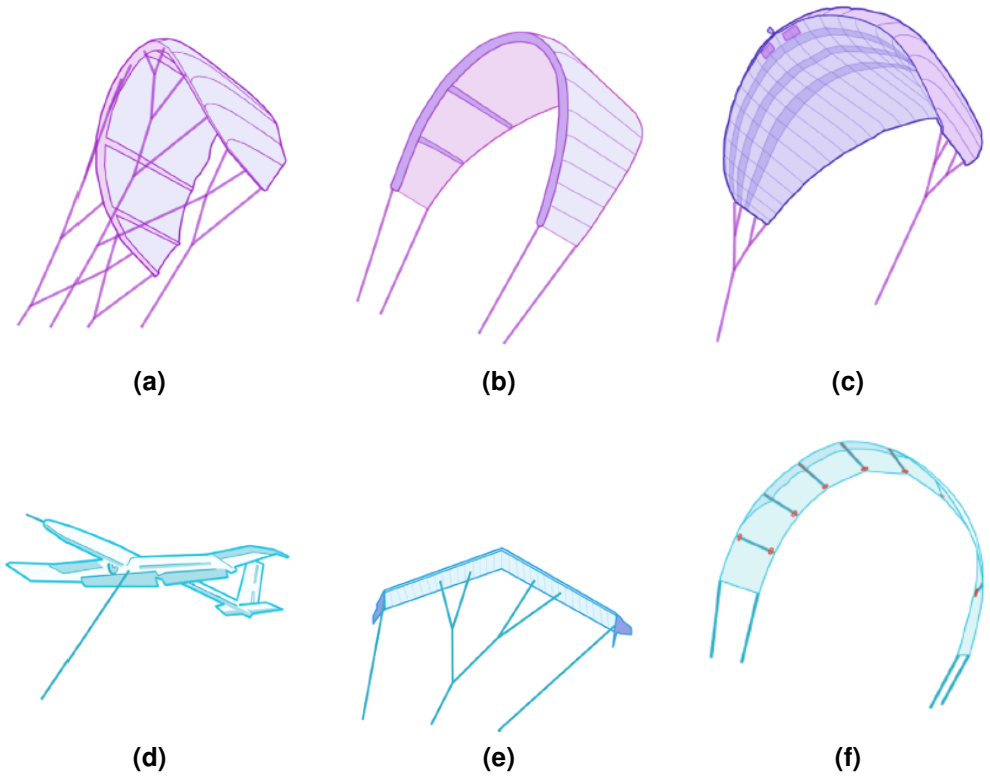

Figure 2.3: *Different airfoil types in AWES. (a) LEI-SLE Kite; (b) LEI-C C kite; (c) Foil Kite; (d) glider; (e) Swept rigid wing; (f) Semi-rigid airfoil.*

Source: Adapted from [10].

Different wing types are exemplified in figure 2.3.

2.1.1 Pumping-kite mode

This work focuses on a specific group of AWES that operates in the pumping kite mode. This is a very common ground generation mode of operation that can be employed using any kind of wing. As already mentioned, AWES that generate energy on the ground require movement of the supporting tether to generate energy. This is achieved by either moving the generation unit or unwinding the tether. There are a few variations of moving base AWES, as in the trajectory of the moving base or its structure. Moving the generation structure makes it difficult to transfer the energy to the grid and can be the source of many problems. Unwinding the tether avoids these problems but creates another one: the need to rewind the tether back at some point. This can be done through a retraction maneuver where the generator on the ground acts as a motor, spending a fraction of the produced energy while the airfoil is positioned to re-

duce the traction force on the cable. After a determined amount of cable is rewinded a new system's operation cycle begins. This strategy is called the pumping kite mode and one cycle of operation is called a pumping cycle, illustrated in figure 2.4.

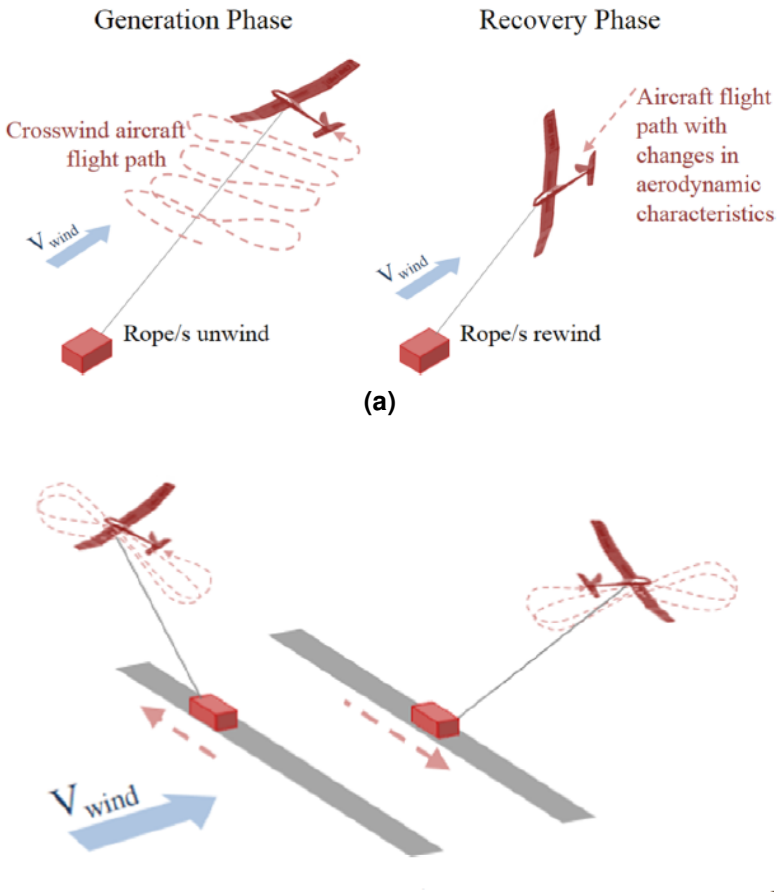

Figure 2.4: *Pumping kite and moving-ground-station AWES*

Source: Adapted from [10]

Through the rest of this document the operating stage where energy is generated and the cable is being unwinded will be refered to as active phase, traction phase or generation phase. The phase where the cable is rewinded will be called passive, retraction or recovery phase.

The kite flight trajectory is very important in both operation stages, making its control an essential part of the system's operation. In the active phase, the airfoil trajectory is defined to maximize the wind mechanical power harvested by the airfoil. In the passive phase, the objective is to reduce the wind power, consequently reducing the traction and making it easier to rewind the cable, however, the traction can not be reduced too much, otherwise the kite would stall and fall.

Equally important as the flight trajectory, the unwinding and rewinding speed of the tether in both stages severely affects flight stability and power generation.

2.2 Modeling

To enable a more in depth understanding of the pumping kite system and also to allow the development of the control and optimization solutions intended in this work it is necessary to study the mathematical modeling of pumping-kite systems.

It is said that a control solution is only as good as the system's model and sensors on which it is based. This statement encourages the use of more accurate models, however, this accuracy is usually consequence of a more complex model and model complexity requires more computational time and complex solutions. The most complex models describe the airfoil's suffered forces and deformations in detail. These models are often used in complex simulations but the high associated computational cost make them unsuited for on-line optimization and control applications [12]. In the case of real-time computations the models must be relatively simple.

2.2.1 Aerodynamics

A fixed aerodynamic profile under a constant velocity airflow $\mathbf{W_e}$ suffers the action of two forces: a lift force ($\mathbf{F_l}$) and a drag force ($\mathbf{F_d}$). The drag force is always in the same direction of the airflow while the lift force is always perpendicular. In aircraft and in ground-generation AWES the lift force is the one explored to produce mechanical work. In this case the drag is undesired and an ideal profile would produce infinite lift and no drag. This concept leads to the notion of aerodynamic efficiency (E), that is expressed as the ratio of the lift force module by the drag force module.

$$E = \frac{\mathbf{F_l}}{\mathbf{F_d}} \tag{2.1}$$

Several effects influence each of these forces making a fully analytical formulation hard to obtain and unpractical to use. In practice these effects are condensed in lift and drag coefficients c_l and c_d that are used to calculate the forces module (F_l and F_d) through equations 2.2a and 2.2b, where ρ is the air density, A is the airfoil projected area and W_e is the effective wind speed module. The effective wind is the actual speed of the wind around the airfoil and can be expressed mathematically as $\mathbf{W_e} = \mathbf{W_n} - \dot{\mathbf{r}}$,

where $\dot{\mathbf{r}}$ is the airfoil velocity.

$$F_l = \frac{1}{2}\rho A c_l(\alpha, u_d) W_e^2 \tag{2.2a}$$

$$F_d = \frac{1}{2}\rho A c_d(\alpha, u_d) W_e^2 \tag{2.2b}$$

The aerodynamic coefficients depend on the angle that the effective wind hits the airfoil. This is expressed by the angle of attack α that is defined relative to the chord line. All of the aforementioned concepts are depicted in figure 2.5. There is commonly an actuation method upon the airfoil such as ailerons or similar techniques. For the purpose of generality, we included a generic actuation named u_d that has an independent effect from α on the aerodynamic coefficients c_l and c_d.

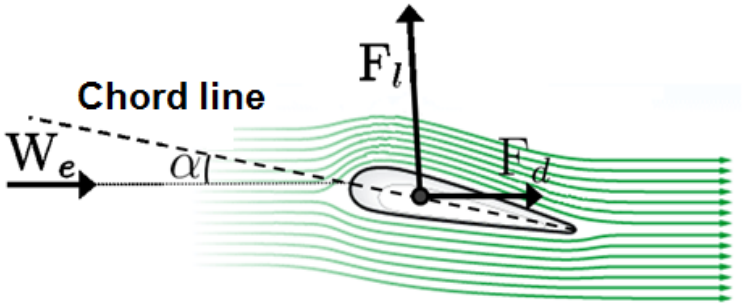

Figure 2.5: *Aerodynimic forces ($\mathbf{F_l}$ and $\mathbf{F_d}$) and angle of attack (α).*

Source: Adapted from [27]

2.2.2 Wind

The study and modeling of wind phenomena is quite complex, making wind speed and direction prediction across the land and at higher altitudes the topic of many researches. In the wind energy scenario the interest is usually on low altitude wind, studying how it changes with altitude and in short periods of time. Wind changes during longer periods of time are also studied in an attempt to predict the energy production capacities of different locations in the future.

In the case of AWE, we assume that the airfoil operates in the atmospheric boundary layer, that extends up to 600 m above ground, in which the logarithmic wind shear model is a good approximation of the wind speed variation with altitude. This model, stated in equation 2.3, depends on three parameters: a reference wind speed v_{ref} at a reference altitude z_{ref} and the surface roughness z_0, that represents the logarithmic

gain with altitude due to air friction with the rough terrain.

$$W_n(z) = V_{ref} \frac{\ln(\frac{z}{z_0})}{\ln(\frac{z_{ref}}{z_0})} \tag{2.3}$$

The shear wind model only captures the variation of the average wind speed with altitude, $W_n(z)$. Since the wind can blow in any direction it needs to be denoted as a vector. We assume that the nominal wind is always parallel to the ground and, since wind generators want to always be aligned to the wind, we define a coordinate system where the x axis is aligned to the nominal wind vector hence the nominal wind is

$$\mathbf{W_n}(\mathbf{z}) = \begin{bmatrix} W_n(z) \\ 0 \\ 0 \end{bmatrix}. \tag{2.4}$$

The actual wind speed relative to the ground is composed by the nominal wind plus disturbances. These disturbances can be modeled to a certain degree by mathematical equations that capture the effect of gusts, however, in this work we will not assume any disturbance models.

Finally, the wind from the perspective of a moving airfoil needs to account for the airfoil's moving speed. This leads to the equation of the effective wind, also called apparent wind. Where $\mathbf{V_k}$ is the airfoil speed and $\mathbf{W_d}$ are the wind disturbances.

$$\mathbf{W_e} = \mathbf{W_n} + \mathbf{W_d} - \mathbf{V_k} \tag{2.5}$$

With this framework the pumping-kite models used for the rest of this work can be introduced.

2.2.3 Point-mass model

This model, presented in [15, 9] is built upon a simpler version published in [13], and aims at describing a tethered airfoil in a pumping-kite configuration by a set of six dynamic states that describe the airfoil's position and velocity in polar coordinates, namely the azimuth angle ϕ, the polar θ angle and the Cartesian distance form the origin l, together with their first-order time derivatives. The airfoil plus control pod is represented as a single equivalent point mass m at Cartesian coordinates $\mathbf{r}$ and subject to aerodynamic, gravitational, apparent, and line traction forces. This point mass is assumed to be anchored to the ground by a rigid segment of variable length $r = \|\mathbf{r}\| = l$, subject to aerodynamic, apparent and gravitational forces only. Additionally, the tether can be modeled as a second point mass at half the total r distance with mass $m_t(r)$

dependent on the tether length. The tether mass is expressed as

$$m_t(r) = (1/4)\rho_t \pi d_t^2 r \tag{2.6}$$

where ρ_t is the is the volumetric mass density of the tether and d_t is its diameter.

Unlike its predecessor, this model considers variations of the aerodynamic coefficients as functions of the airfoil's angle of attack, leading to more realistic results.

More specifically, this model initially defines two reference frames: the *inertial* reference frame $(\mathbf{e}_x, \mathbf{e}_y, \mathbf{e}_z)$, which is centered at the system anchorage point on the ground, and whose $\mathbf{e}_x$ and $\mathbf{e}_z$ axes are aligned with the nominal wind vector $\mathbf{w}_n^i = [w_{nx}, 0, 0]^T$ and with the negative of the gravity vector $\mathbf{g}$, respectively; the *local* reference frame $(\mathbf{e}_\theta, \mathbf{e}_\phi, \mathbf{e}_r)$, centered at the aircraft center of gravity and whose axes are defined as $\mathbf{e}_\theta = \frac{\partial \mathbf{r}}{\partial \theta}\frac{1}{r}$, $\mathbf{e}_\phi = \frac{\partial \mathbf{r}}{\partial \phi}\frac{1}{r\sin\theta}$, and $\mathbf{e}_r = \mathbf{e}_\theta \times \mathbf{e}_\phi$. $\mathbf{r}$ is defined in the inertial frame as

$$\mathbf{r} = \begin{bmatrix} r\sin\theta\cos\phi \\ r\sin\theta\sin\phi \\ r\cos\theta \end{bmatrix}. \tag{2.7}$$

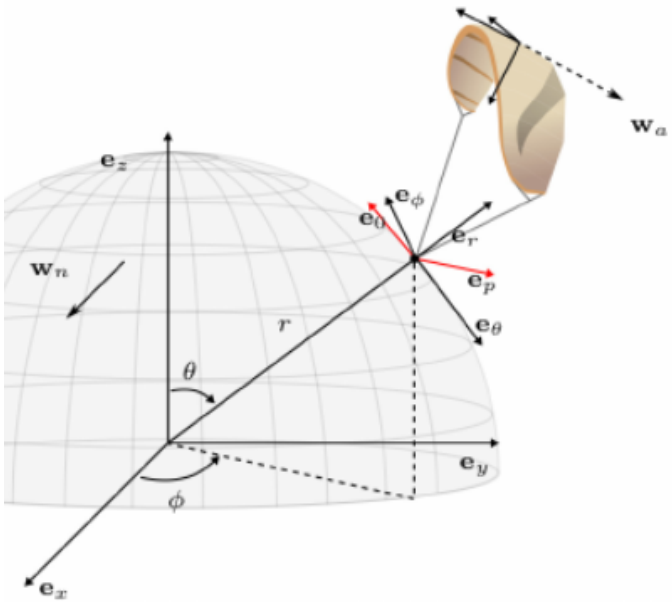

Figure 2.6: *Representation of inertial and local coordinate systems.*

Source: Adapted from [29]

The aforementioned coordinate systems are depicted in figure 2.6.

Note that the unit vectors $(\mathbf{e}_\theta, \mathbf{e}_\phi, \mathbf{e}_r)$ in the inertial frame are the columns of the rotation matrix that rotates from inertial to local frames

$$\mathcal{R}_i^l = \begin{bmatrix} \mathbf{e}_\theta & \mathbf{e}_\phi & \mathbf{e}_r \end{bmatrix} = \begin{bmatrix} \cos\theta\cos\phi & \cos\theta\sin\phi & -\sin\theta \\ -\sin\phi & \cos\phi & 0 \\ \sin\theta\cos\phi & \sin\theta\sin\phi & \cos\theta \end{bmatrix}. \tag{2.8}$$

The kite speed is expressed in the local frame as

$$V_k^l = [r\dot{\theta}, r\dot{\phi}\sin\theta, \dot{r}]^T \tag{2.9}$$

A simple and elegant way to derive the equations of motion is to use Lagrangian mechanics, where the configuration of a system is described by an arbitrary, independent set of generalized coordinates $\mathbf{q} \in \mathbf{Q}$. Since the tether length constraint is inherently considered in the polar coordinate system, the Lagrange function of the system is defined as

$$\mathscr{L}(\mathbf{q}, \dot{\mathbf{q}}) = T(\mathbf{q}, \dot{\mathbf{q}}) - V(\mathbf{q}) \tag{2.10}$$

where $T(\mathbf{q}, \dot{\mathbf{q}})$ is the kinetic energy of the system as function of its generalized coordinates and their derivatives, and $V(\mathbf{q})$ represents its potential energy as function of the generalized coordinates at any time instant.

The Lagrange function applied to the model proposed in polar coordinates is expressed as

$$T(\mathbf{q}, \dot{\mathbf{q}}) = \frac{1}{2}(m + \frac{1}{4}m_t)[\dot{r}^2 + r^2(\dot{\theta}^2 + \dot{\phi}^2\sin^2\theta] \tag{2.11a}$$

$$V(\mathbf{q}) = (m + \frac{1}{2}m_t)gr\cos\theta \tag{2.11b}$$

From this point the equations for $\ddot{\theta}$, $\ddot{\phi}$ and $\ddot{r}$ can be obtained by soling the Euler-Lagrange equation

$$\frac{d}{dt}\frac{\partial\mathscr{L}}{\partial\dot{\mathbf{q}}} - \frac{\partial\mathscr{L}}{\partial\mathbf{q}} = \mathbf{F}_q \tag{2.12}$$

for each q_i coordinate, where $\mathbf{F}_q$ is the vector of generalized forces acting on the system, i.e. the aerodynamic forces. We arrive at the general expression for the model equations:

$$\begin{aligned} \ddot{\theta} &= \frac{1}{m_{eq}r}[(m + \frac{1}{2}m_t)g\sin\theta - 2m_{eq}\dot{r}\dot{\theta} - \sum \mathbf{F}_{ext}^{\theta}] \\ \ddot{\phi} &= \frac{1}{mr\sin\theta}[-2m_{eq}\dot{\phi}(\dot{r}\sin\theta + r\dot{\theta}\cos\theta) - \sum \mathbf{F}_{ext}^{\phi}] \\ \ddot{r} &= \frac{1}{m}[-(m + m_t)g\cos\theta + m_{eq}r(\dot{\theta}^2 + \dot{\phi}^2\sin^2\theta) - \sum \mathbf{F}_{ext}^{r}] \end{aligned} \tag{2.13}$$

In the equations above, $\mathbf{F}^{\theta}_{ext}$, $\mathbf{F}^{\phi}_{ext}$ and $\mathbf{F}^{r}_{ext}$ are the components of the external forces on each spheric coordinate, and $m_{eq} = (m + \frac{1}{4}m_t)$.

For the rest of the derivation analytical expressions for the external forces need to be derived. Since the motion in the azimuth direction is ignored in this work, the rest of the derivation will assume the airfoil is operating in the $\phi = 0$ plane, reducing the state space to θ, l and its first time derivatives.

The only external forces acting up on the airfoil are the aerodynamic forces and the tether traction. The tether traction acts only in the direction of $\mathbf{e_r}$, since the tether is assumed to be a perfect line, and can only be negative since a positive traction would mean that the tether is pushing the airfoil. This is depicted in figure 2.7. To fully express the model it is necessary to arrive at a expression for the aerodynamic forces acting on the airfoil and the tether. The effective wind can now be fully expressed in a given state considering no disturbance as

$$W_e^l = \mathbf{W_n^l}(z) - \mathbf{V_k^l} = \begin{bmatrix} \cos\theta W_n - r\dot{\theta} \\ \sin\theta W_n - \dot{r} \end{bmatrix} \tag{2.14}$$

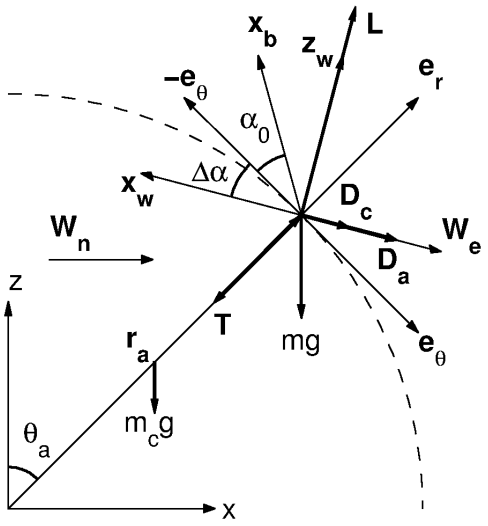

Figure 2.7: *Different forces acting on the airfoil*

Source: Adapted from: [28]

The angle of attack can be defined as

$$\alpha = \alpha_0 + \triangle\alpha = \alpha_0 + atan\left(\frac{W_{e[r]}}{W_{e[\theta]}}\right) \tag{2.15}$$

Where α_0 is the angle from the airfoil chord line to the plane perpendicular to $\mathbf{e_r}$, as shown in figure 2.8. This angle is defined by the airfoil structure and can be either fixed

or variable, providing way to manipulate indirectly the aerodynamic forces. In this work we will consider a fixed α_0 since a different control input will be used to affect these forces.

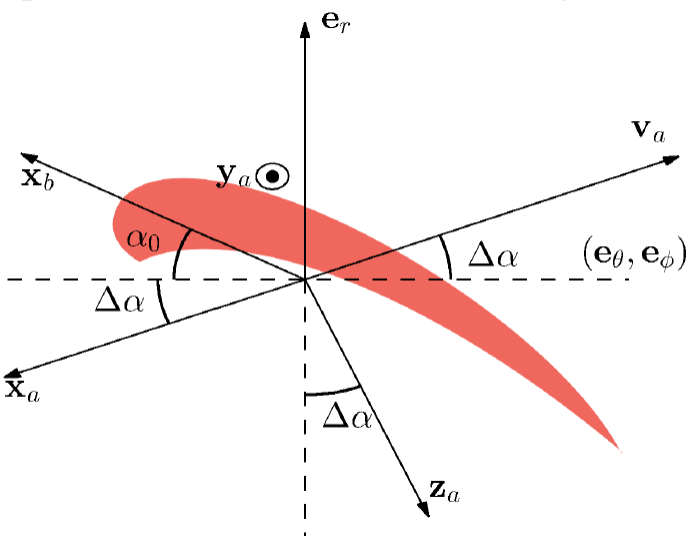

Figure 2.8: *Decomposition of airfoil angle of attack.*

Source: [12]

Finally the airfoil lift and drag forces can be calculated using equations 2.2a and 2.2b. leaving only the cable aerodynamic forces left to be calculated. While the cable lift is negligible its drag can have a huge influence on the flights dynamics, mainly when flying at high speeds. The tether drag force influence on the airfoil is expressed as

$$F_d, t = \frac{1}{8}\rho A_t c_{d,t} W_e^2 \tag{2.16}$$

with $A_t = r d_t \cos\Delta\alpha$ being the tether area projection perpendicular to the wind and $c_{d,t}$ the tether drag coefficient. Considering the kite and the tether drag one can formulate a equivalent drag coefficient $c_{d,eq}$ for the tether-airfoil system, defined as

$$c_{d,eq}(\alpha, u_d) = c_d(\alpha, u_d) + \frac{n_t c_{d,t} r d_t cos(\Delta\alpha)}{4A} \tag{2.17}$$

With the perfectly stiff tether assumption the airfoil efficiency can be defined as $E = c_l/c_{d,eq}$.

We can now state the complete form of the equations of motion:

$$\ddot{\theta} = \frac{1}{m_{eq} r}[(m + \frac{1}{2}m_t)g\sin\theta - 2m_{eq}\dot{r}\dot{\theta} + \frac{1}{2}\rho A W_e^2(-c_l(\alpha, u_d)\sin\Delta\alpha + c_{d,eq}(\alpha, u_d, r)\cos\Delta\alpha)]$$
$$\ddot{r} = \frac{1}{m}[-(m + m_t)g\cos\theta + m_{eq} r\dot{\theta}^2 + \frac{1}{2}\rho A W_e^2(c_l(\alpha, u_d)\cos\Delta\alpha + c_{d,eq}(\alpha, u_d, r)\sin\Delta\alpha) - T_t] \tag{2.18}$$

In equation 2.18, the tether traction T_t is a manipulated variable. However, in many cases the tether acceleration is manipulated, in which case T_t and $\ddot{r}$ switch sides in equation 2.18.

2.2.4 The point-mass wing in dynamic equilibrium

The previously described model models the dynamical behavior of the system. However there are many relations that are already accounted for in the dynamical equilibrium of the airfoil, where it moves at constant speed. This motivates the use of simpler, in-equilibrium model, that can be used for optimization purposes. This model has been presented in [31] and expanded in many works, including [12], and [15].

When suffering no acceleration, the forces acting on the airfoil, represented in figure 2.7, cancel each other. The analysis on each local coordinate decomposition leads to the two following equations

$$\begin{aligned} F_l \sin\Delta\alpha - F_d \cos\Delta\alpha = 0 \\ F_l \cos\Delta\alpha + F_d \sin\Delta\alpha - T = 0 \end{aligned} \tag{2.19}$$

In these equations, the weight force is being disregarded, which usually has very low values relative to the aerodynamic forces. Replacing the expression of the aerodynamic forces presented in equations 2.2a and 2.2b and the expression of the effective wind from equation 2.14 a simplified equation for the tether traction in equilibrium at zero azimuth is found

$$T = \frac{1}{2}\rho A c_l \frac{1}{E}\left(1 + \frac{1}{E^2}\right)^{\frac{3}{2}}(W_n \sin\theta - \dot{r})^2 \tag{2.20}$$

By solving equations 2.19 one can find the dynamic share of the angle of attack:

$$\Delta\alpha = arg\left\{c_l(\Delta\alpha + \alpha_0) * \sin\Delta\alpha - c_{d,eq}(\Delta\alpha + \alpha_0, r) * \cos\Delta\alpha = 0\right\} \tag{2.21}$$

2.3 The UFSCKite System

The UFSCKite prototype, focus of this work, is a pumping kite mode AWES of 12KW rated power that uses a foil kite. In this section the many aspects of the system will be presented, from the prototype structure and the actuation and measurement hardware to the control and filtering system. It is important to highlight that the choice of control strategy and instrumentation were not part of this work, but was already made by engineers of the UFSCkite group.

2.3.1 Actuation

The kites in pumping kite mode systems usually have two actuation mechanisms: one to affect the airfoil's steering, to make curves, and other that reduces the system's aerodynamic efficiency, enabling a reduction on the cable's traction. This last actuation is usually refered to as "depower" and was previously denoted as u_d. The working principle behind these actuations varies for different wing types. For rigid wings it may be used structures similar to airplane's ailerons that change the base angle of attack α_0, whereas in flexible wings it is usually achieved by deforming the airfoil structure which alters the aerodynamic coefficients. Since the system considered in this work uses a foil kite, the steering and depower actuations will be further explained for this specific type of airfoil.

In foil kites, there are usually cables connected to four regions in the airfoil called lines. The three lines in the "front", near the leading edge exert a stronger traction on the cables while the back line, called F-line, see figure 2.9, exerts a smaller force, thus offering a smaller resistance to the intended actuations on the airfoil [12].

The cables connected to the F-line are control cables of variable length. They can be released or pulled either differentially, to give a a steering command, or together, to have a depower effect.

Motors are necessary to pull or release the control cables. In the presented system, these motors are located in a control module that flies close to the airfoil and to which are connected all the tethers of the airfoil. This scheme allows for a single traction tether to be used to connect the control module, also called control pod, to the generator on the ground and, as the actuation tethers can be smaller, it allows for faster actuation. On the other hand, the flying control unit adds weight and complexity to the system besides requiring an energy source to power it. Alternatively, the control and traction tethers could all be attached directly to a single control unit on the ground. The disadvantages of such alternative is the drag produced by the extra cables and the additional actuation delay. Both schemes are depicted in figure 2.10.

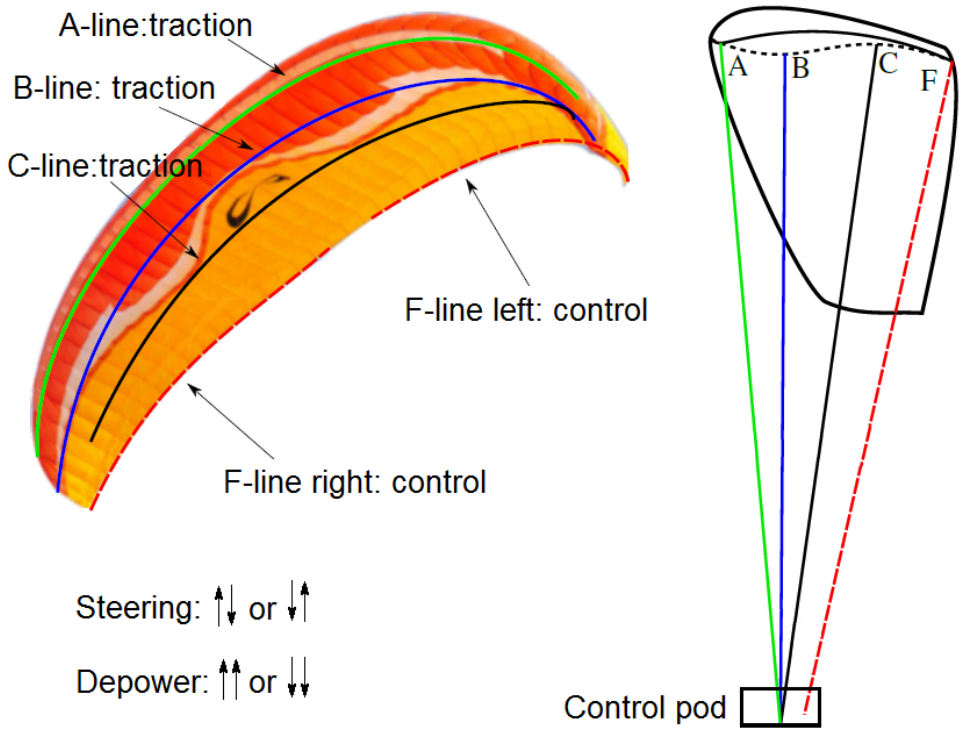

Figure 2.9: *Attachment lines to the airfoil and control lines position.*

Source: Adapted from [12]

2.3.2 Measurement

The measurement scenario in AWES is quite diverse with many solutions still being explored. The UFSCKite system during the development of this work has measurement information of the following physical quantities: tether length, speed and acceleration, kite position, main tether traction and wind speed.

The tether's position, speed and acceleration can be directly obtained from the digital inverter that controls the ground unit motor/generator. To achieve better precision an external encoder is used on the motor's rotation axis.

The kite position is measured indirectly through two measurements: the main tether's direction and length and a radio frequency triangulation system. In the first case, two encoders measure the angles of the tether relative to a reference direction in the ground plane. To calculate the kite position from this information the cable is considered to be perfectly stretched in a line. In reality the tether presents a small curve due to its weight and the aerodynamic drag that it suffers, but the assumption is a good approximation if the tether is under a sufficiently high traction. The radio frequency triangulation system measures the distance of the kite to four anchor points in the ground using the round trip time of radio signals from the anchor points to a radio module attached to the kite.

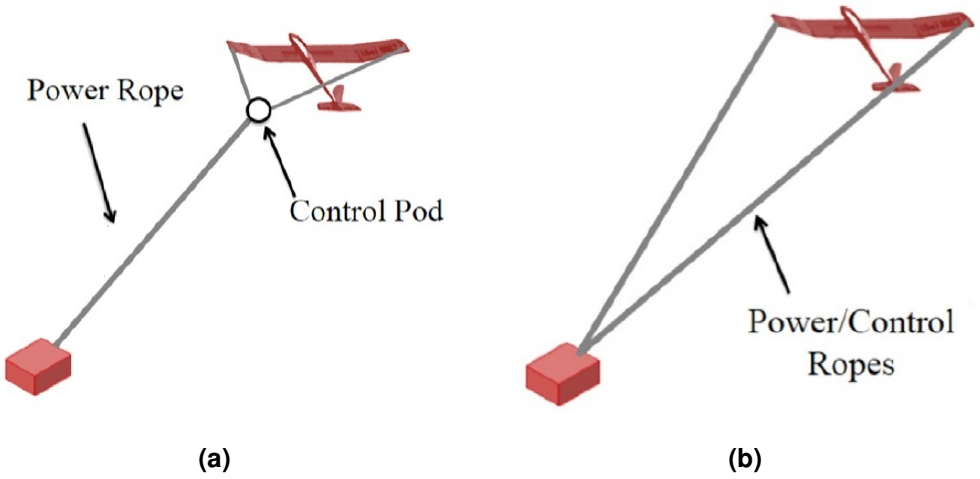

Figure 2.10: *AWES control using (a) a control pod and (b) through the power tethers.*

Source: Adapted from [10]

This second system is still under experimentation phase but it provides a more exact measurement since it is not influenced by the tether curve.

The tether's traction is measured using load cells, being simple and efficient.

The wind speed is measured with an off-the-shelf anemometer at a reference altitude. This measurement is then used as reference wind speed (W_{ref}) at a reference height (z_{ref}). Besides the wind speed, the anemometer also provides the wind direction on the ground plane. Note that a measurement of the wind at the kite's altitude is not available. This, among other reasons to be mentioned, motivates the need of a filtering strategy to determine model parameters.

2.3.3 Filtering

Filtering can be employed for different purposes in a AWES but the two most significant applications are fusing sensor data to provide a more reliable position and velocity data, and estimating diverse system parameters.

This works was developed considering that the filtering algorithms of the target system are able to provide an estimation of the aerodynamic coefficients depending on the airfoil's angle of attack and its depower actuation, besides also estimating the current angle of attack. Since such filtering algorithm was not available at the time this work was developed the aerodynamic coefficient surfaces were built using curves borrowed from the literature for the variation with respect to the angle of attack and adding a sigmoid curve factor to the depower actuation, yielding the surface shown in figure 2.11

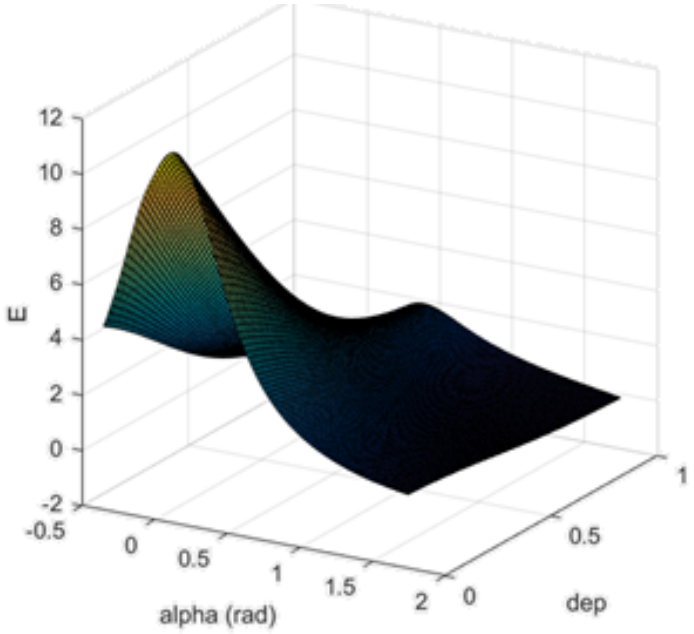

Figure 2.11: *AWES Aerodynamic efficiency as a function of the angle of attack (alpha) and the depower actuation (dep).*

Source: Original

2.3.4 Control architecture

While all other topics covered in this section influence the work developed the control architecture already employed by the UFSCKite group is certainly what influences the most, since the solution proposed in this work should be compatible with the UFSCKite prototype. The architecture employed follows a decentralized control strategy, where the flight path and the tether length of the system are controlled locally.

The steering command is computed to make the kite follow a predefined lemniscate trajectory through a course angle controller. The full design of this system can be studied in [12]. Separately, the reeling speed of the winch is manipulated to impose an off-line generated traction trajectory by a traction control system. At last, the depower reference is generated together with the the traction trajectory and is directly applied by the servomotors.

The use of a decentralized control approach allows for the design of controllers with faster processing times and overall better results. The reference generation is closely related to the airfoil's trajectory in space and is where the solution proposed in this work fits the control architecture.

Solutions currently found in the literature are able to generate off-line optimized references for tether traction, depower actuation and kite trajectory parameters. The

main problem for this approach is that the off-line calculated trajectories are optimized for a given nominal wind condition and for a expected set of system parameters.

The kite trajectory parameters previously mentioned are the parameters that define a fixed lemniscate shaped trajectory. This target trajectory defines course angle reference, a variable based on which the steering input is computed. The course angle is the direction of the kite movement on the $\mathbf{e}_\theta \mathrm{x} \mathbf{e}_\phi$ plane.

Chapter 3

Related Work and theoretical background

The main points of study required for the development of this work were AWES, previous works of optimization of pumping-kite systems and general optimization and predictive control. Since this is the first work in the UFSCKite group to attempt to use predictive control for a pumping-kite system and the first experience of the author with optimization and predictive control, there was a lot to be covered. This chapter attempts to condense the most essential information in two sections, one to cover the required knowledge of predictive control and optimization, and another to review the strategies adopted in previous works.

3.1 Nonlinear model based predictive control

Model predictive control (MPC) is an advanced control technique that has reached a high number of industrial processes since its initial adoption. The general idea behind this class of controller is to use a mathematical model to predict the dynamical behavior of a system and calculate a control action that minimizes a chosen cost or objective function. From this general idea, the different MPC techniques vary in three main aspects:

- The prediction Model
- The objective function
- The method to obtain the control law

The most widely used MPC techniques, the Dynamical Matrix Control (DMC) and the General Predictive Control (GPC), use linear models based on the step response and transfer functions, respectively, and use a very similar objective function and control law formulation. The most common cost function is composed of a tracking error penalization factor and a control variation penalization factor. These factors are

weighed for each future discrete sample time in a finite prediction horizon of N samples where N is expressed by a beginning sample N_1 and an ending sample N_2, with $N = N_2 - N_1 + 1$. The future control increments are calculated up to $N_u \in \{1, 2, 3, ..., N_2\}$ samples. The cost function is then expressed as

$$J(\mathbf{\Delta u}) = \sum_{j=N_1}^{N_2} \delta(j)[\hat{y}(t+j|t) - w(t+k)]^2 + \sum_{j=1}^{N_u} \lambda(j)[\Delta u(t+j-1)]^2$$

For MIMO systems there is a $\delta_\mathbf{i}$ weight vector for each controlled variable $\mathbf{y_i}$ and a $\lambda_\mathbf{i}$ weight vector for each manipulated variable increment $\mathbf{\Delta u_i}$. Similarly, in the multivariable case, different control and prediction horizons can be defined for each variable.

The optimal control vector is calculated for the entire control horizon N_u, however, only the first control is applied. After that, the horizon is shifted and fed with new measurements from the system. This is called the receding horizon strategy.

The quadratic form of the cost function leads to good convergence properties of numerical methods and even to a known analytical solution given by the Linear-Quadratic Regulator (LQR). This solution, however, is for the unrestricted case with an infinite horizon. By using a quadratic programming solver, the solution subject to a set of linear restrictions given by $A\mathbf{\Delta u} \leq \mathbf{b}$ and $A_{eq}\mathbf{\Delta u} = \mathbf{b_{eq}}$ is found.

From these classical methods many variations and sophistications have been presented. Since most real processes are inherently non-linear, linearization techniques are used to obtain the model. For many processes this procedure is acceptable, because the linearized model represents the system very well around the linearization point. For other processes, however, a more complex representation is necessary.

According to [25] there are three main different approaches for nonlinear model predictive control:

- MPC with non-linear prediction models on the objective function
- Methods based on particular models
- Methods based on linearization

The first approach is perhaps the most natural as it attempts to use the non-linear model equations to directly derive the objective function. This approach uses nonlinear optimization methods such as interior-point methods (IP) or sequential quadratic programming (SQP). The receding horizon characteristic is maintained but the optimization problem to be resolved in each time step adopts a more general form

$$\begin{aligned} \underset{\mathbf{u}}{\text{minimize}} \quad & f(\mathbf{W}, \mathbf{Y}, \mathbf{u_p}, \mathbf{u}) \\ \text{subject to} \quad & h(\mathbf{u}) = 0 \\ & g(\mathbf{u}) \leq 0 \end{aligned}$$

where $\mathbf{W}$ is the future reference vector, $\mathbf{Y}$ the vector with future and past controlled variables, $\mathbf{u_p}$ the past control variables and $\mathbf{u}$ the present and future control variables. Besides that, f needs to have a single output and f, h and g need to be continuous and at least two times differentiable.

The second approach uses particular non-linear models to approximate the real model, like Volterra Series or Hammerstein models [26] [7]. This may be interesting if the selected models are a good approximation for the system as they may facilitate the optimization process.

The third approach consists in using a linearized version of the model for the controller synthesis. Usually these formulations encompass linearization at multiple operation points of the system and a modeling error treatment technique. Another approach is to linearize the system at every sample period, by replacing the nonlinear problem with a sequence of linear problems, achieving simplification but not guaranteeing optimality or convergence [18].

The first model predictive controllers to be applied in AWES employed the first approach using the non-linear models directly to predict the system. The most recent successful approaches have come closer and closer to successive linearization approach described last. For this reason, the next sections describes briefly the general formulation of non-linear optimal control problems, an adaptation of this class of problem for real-time solution, as a MPC technique, and finally a practical non-linear MPC as in [25] is presented.

3.1.1 Optimal control problems

Just like the general idea of MPC, optimal control problems (OCP) use a system model and a given cost function to calculate the future control actions that minimize the cost function. Unlike the MPC, this more general class of problems are not designed to be applied online and calculated at every step. This section is heavily based in the summary presented in [17] and does not cover in detail the inner works of the optimization algorithms employed. The focus of the section is to state how these optimization problems are defined to later show how a NMPC approach is derived.

Optimal control problems usually define an optimization problem that falls in the class of nonlinear programming (NLP), a particular class of problems in the continuous

optimization class of problems that fits the following formulation:

$$\begin{aligned} \underset{\mathbf{w}\in\mathbb{R}^{\mathrm{n}}}{\text{minimize}} \quad & f(\mathbf{w}) \\ \text{subject to} \quad & h(\mathbf{w}) = 0 \\ & g(\mathbf{w}) \leq 0 \end{aligned}$$

where $f : \mathbb{R}^{\mathrm{n}} \to \mathbb{R}$, $g : \mathbb{R}^{\mathrm{n}} \to \mathbb{R}^{\mathrm{m}}$ and $h : \mathbb{R}^{\mathrm{n}} \to \mathbb{R}^{\mathrm{p}}$.

OCP usually are based in state-space representation of systems. Where the system is fully represented by a set of state variables such that its dynamical behavior is described by the first time derivative of these variables and is affected by control inputs $u(t)$ and disturbances $q(t)$.

$$\dot{\mathbf{x}}(t) = \Phi(\mathbf{x}(t), \mathbf{u}(t), \mathbf{q}(t))$$

Since most real life processes are continuous one may implement a continuous optimal control problem, or calculate a discrete equivalent of the system and build a discrete optimal control problem. For continuous optimal control problems, however, the most successful approach has been direct methods that replace the continuous problem into a discrete and finite non-linear problem.

Discrete optimal control

Discrete systems are usually periodically sampled continuous systems such that the time evolution depends on an integer representing the sample number that implicitly multiplies the sample period. Discrete system dynamics can be modeled by an update law such as:

$$\mathbf{x_{k+1}} = \Phi_k(\mathbf{x_k}, \mathbf{u_k}, \mathbf{q_k}), k = 0, 1, 2, ..., N-1$$

Where once again the concept of prediction horizon is employed. A generic cost function can be defined for NLP of a general discrete OCP, with a term $L(\mathbf{x_k}, \mathbf{u_k})$ that is evaluated for every sample time within the prediction horizon and a $E(\mathbf{x_N})$ term that penalizes the final state differently. These terms are commonly denominated stage cost and final cost, respectively. The NLP then solves for both the values of control inputs and the controlled variables in every sample time in the horizon while ensuring the dynamic constraints imposed by the dynamical equations of the system.

$$
\begin{aligned}
&\underset{\mathbf{x_0},\mathbf{u_0},\mathbf{x_1},...,\mathbf{u_{N-1}},\mathbf{x_N}}{\text{minimize}} && \sum_{k=0}^{N-1} L(\mathbf{x_k},\mathbf{u_k}) + E(\mathbf{x_N}) \\
&\text{subject to} && \mathbf{x_{k+1}} - \Phi(\mathbf{x_k},\mathbf{u_k}) = 0, \quad k = 0,...,N-1; \\
& && h(\mathbf{x_k},\mathbf{u_k}) \leq 0, \quad k = 0,...,N-1; \quad r(\mathbf{x_0},\mathbf{x_N}) \leq 0.
\end{aligned}
$$

Besides the dynamical equations of the system, it is also included general path constraints h at boundary conditions imposed by r. Path constraints ensure general constraints like control variable saturations, skew rate saturation, overshoot requirements, etc while boundary conditions may include periodicity constraints, i.e. $x_0 = x_N$, fixed initial states and set-points.

Continuous optimal control

Conceptually the continuous OCP formulation is analogous to discrete OCP but the states and manipulated variables evolve in the continuous domain. This way, the stage cost is evaluated in a integral and optimization horizon is expressed in a continuous time interval $[0, T]$, resulting in the following NLP

$$
\begin{aligned}
&\underset{\mathbf{x}(.),\mathbf{u}(.)}{\text{minimize}} && \int_0^{N-1} L(\mathbf{x}(t),\mathbf{d}(t))\mathrm{d}t + E(\mathbf{x}(T)) \\
&\text{subject to} && \dot{\mathbf{x}}(t) - \Phi(\mathbf{x}(t),\mathbf{u}(t)) = 0, && t \in [0,T]; \\
& && h(\mathbf{x}(t),\mathbf{u}(t)) \leq 0, && t \in [0,T]; \\
& && r(\mathbf{x}(0),\mathbf{x}(T)) \leq 0.
\end{aligned}
$$

As commented before, one of the most successful methods for solving an OCP are the called direct methods. The idea behind these methods is to use numerical simulation methods in a discrete and defined time grid $0 = t_0 \leq t_1 \leq t_2 \leq ... \leq t_N = T$, where $t_{k+1} - t_k = t_k - t_{k-1}$ is not necessarily true. As a result, the infinite set of decision variables $\mathbf{x}(t)$ and $\mathbf{u}(t)$ is reduced to a finite amount $\mathbf{x}_k$ and $\mathbf{u}_k$ that represent the previous set at the discretization nodes. The constraints are also evaluated only at the discretization nodes completely transforming the previous continuous OCP into a discrete OCP formulation.

Within the direct methods there are still different methods to discretize the continuous dynamics. Here will be presented two of the most common methods: single shooting and multiple shooting. Another common construction that will not be presented here is the direct collocation.

Single shooting

The single shooting method models the control $\mathbf{u}(t)$ by piece-wise polynomials in the time grid defined by $0 = t_0 \leq t_1 \leq t_2 \leq ... \leq t_N = T$. The most common modeling is piece-wise constant control so the control is defined as $\mathbf{U} = (\mathbf{u}_0, \mathbf{u}_1, ..., \mathbf{u}_{N-1})$, with $\mathbf{u}_k$ constant in the interval $[t_k, t_{k+1}]$. In this way the states $\mathbf{x}(t)$ can be defined by a numerical integration algorithm, the initial state $\mathbf{x}_0$ and the controls $\mathbf{U}$, being written as $\mathbf{x}(\mathbf{x}_0, t, \mathbf{U})$. As a result, the general continuous OCP can be completely rewritten as

$$\begin{aligned} \underset{\mathbf{x}_0, \mathbf{U}}{\text{minimize}} \quad & \int_0^{N-1} L\left(\mathbf{x}(\mathbf{x}_0, t, \mathbf{U}), \mathbf{U}\right) + E\left(\mathbf{x}(\mathbf{x}_0, t_N, \mathbf{U})\right) \\ \text{subject to} \quad & h\left(\mathbf{x}(\mathbf{x}_0, t_k, \mathbf{U}), \mathbf{u}_k\right), \mathbf{u}_k \leq 0, \ k = 0, 1, ..., N-1; \\ & r\left(\mathbf{x}(\mathbf{x}_0, t_N, \mathbf{U})\right) \leq 0. \end{aligned}$$

Multiple shooting

The multiple shooting method, initially proposed in [8], models the control as a piece-wise polynomial in the same way that the single shooting method does. The difference between the methods is how the multiple shooting method treats the state variables discretization. Instead of modeling it as a function of the initial state and the controls, it leaves the state variables at the discretization nodes as a decision variable for the NLP and numerically integrates the dynamic equation to restrain the calculated solution to a set that respects the systems dynamic equations.

$$\Phi_k(\mathbf{x}_k, \mathbf{u}_k) - \mathbf{x}_{k+1} = 0$$

Finally, the stage cost factor of the objective function is approximated by the cost at each discretization node that approximates the integral of the original stage cost from $[t_k, t_{k+1}]$:

$$\int_0^{N-1} L(\mathbf{x}(t), \mathbf{d}(t))dt = \sum_0^{N-1} \int_{t_k}^{t_{k+1}} L(\Phi_k(t_{k+1}, \mathbf{x}_k, \mathbf{u}_k), \mathbf{d}(t))dt = \sum_0^{N-1} l_k(\mathbf{x}_k, \mathbf{u}_k)$$

Giving the final NLP below.

$$
\begin{aligned}
\underset{\mathbf{x}_0,\ldots\mathbf{x}_N,\mathbf{U}}{\text{minimize}} \quad & \sum_{0}^{N-1} l_k(\mathbf{x}_k,\mathbf{u}_k) + E\left(\mathbf{x}_N\right) \\
\text{subject to} \quad & \mathbf{x}_0 - \overline{\mathbf{x}}_0 = 0, \\
& \Phi_k(\mathbf{x}_k,\mathbf{u}_k) - \mathbf{x}_{k+1} = 0, \quad k = 0,1,...,N-1, \\
& h\left(\mathbf{x}_k,\mathbf{u}_k\right),\mathbf{u}_k \leq 0, \quad k = 0,1,...,N-1, \\
& r\left(\mathbf{x}_N\right) \leq 0.
\end{aligned}
$$

The first constraint determines the system initial condition and the last one can ensure zero reference tracking error, for example.

3.1.2 Online optimization problem

The OCPs presented so far can all be used to build a PNMPC with some sort of adaptation. The discretized time intervals would be required to have a fixed time step and the receding horizon procedure would have to be followed, solving the OCP at every sample time with updated measurements and applying only the present manipulated variables calculated. However, a concern that was not previously present arises: the need to solve the OCP as fast as possible. Solving the OCP faster means that a smaller sample period can be used enabling the control system to react faster to unknown disturbances.

Many works in the AWE community use an algorithm that adapts a nonlinear optimization algorithm into a a real-time NMPC. The algorithm, that will be briefly explained here, is commonly addressed as the real-time iteration scheme.

This scheme adapts the Sequential Quadratic Programming (SQP) optimization algorithm, that solves a sequence of optimization subproblems, each of which optimizes a quadratic model of the objective subject to a linearization of the constraints. However, instead of optimizing multiple subproblems in one MPC iteration, the real-time iteration scheme solves only one subproblem at each MPC iteration and takes advantage of the shifting horizon concept to have enough time to find a solution for the nonlinear problem. This is only possible when using shift initialization, that is, when using the shifted solution of the previous MPC iteration as the initial guess for the optimization problem of the current iteration. With that, the current solution has already been solved for multiple times since the current time entered the prediction horizon.

When using the shift initialization it is necessary to guess a value for the last sample time of the horizon, since it has not been solved for previously. The most simple and effective method to obtain a good initial guess is to just repeat the last value of the previous horizon. This is even more effective when the decision variables are under

variation constraints, limiting the real solution to the vicinity of the guess.

3.1.3 PNMPC

The approach previously presented to NMPC is originated in general optimal control problems and adapted for an on-line controller case. That resulted in a control strategy very different from the classical MPC algorithms. A second approach was studied that is more closely related to the classical MPC techniques, allowing to apply the extensive knowledge, variations and techniques of the linear case to the non-linear case.

In this section, the practical non-linear model predictive control (PNMPC) technique proposed in [25] based on the linearization of the system at every sample period will be presented, together with some techniques that can be used to compensate model mismatch and improve model robustness.

The PNMPC technique was developed directly in the discrete domain and uses the concept of free and forced response used in the GPC and DMC techniques. This divides the system response in two parts: the response due to the previous control inputs, keeping the future control signal constant, and the response due to future variations of the control signal.

This separation is always valid for linear time invariant systems by the principle of superposition. In this case, the vector of predicted variables within a prediction horizon N is given by

$$\hat{\mathbf{Y}} = \mathbf{F}(\overrightarrow{\mathbf{U}}, \overrightarrow{\mathbf{Y}}) + G\Delta\mathbf{u}$$

Where $\overrightarrow{\mathbf{U}}$ is the vector of previous manipulated variables and $\overrightarrow{\mathbf{Y}}$ the vector of previous controlled variables. $\Delta\mathbf{U}$ represents the present and future increments of the manipulated variables within the control horizon N_u. The expression for the free response can be rewritten using the state variables of the system instead of the previous controlled and manipulated variables.

In the most general case, the non-linear dynamic equations of the system can be used to rewrite any system dependent on a process variable u to a dependency on an u_0 and a Δu vector. The non-linear state space representation is

$$\mathbf{y}_k = f(\mathbf{x}_k)$$

$$\mathbf{x}_k = \Phi(\mathbf{x}_{k-1}, \mathbf{u}_{k-1})$$

where $\mathbf{y}_k$, $\mathbf{x}_k$ and $\mathbf{u}_k$ may represent a single or multiple control, state and ma-

nipulated variables, respectively. From these equations the predictions $\hat{\mathbf{y}}_{k+j}$ for $j = 1, 2, ..., N$ can be rewritten as

$$\hat{\mathbf{y}}_{k+j} = f(\Phi(...\Phi(\Phi(\mathbf{x}_{k-1}, \Delta\mathbf{u}_k), \Delta\mathbf{u}_{k+1}), ...), \Delta\mathbf{u}_{k+j-1}) = \Phi^*(\mathbf{x}_k, \Delta\mathbf{U})$$

The PNMPC technique proposes to approximate the Φ^* function by its first order Taylor series approximation. This allows for the vector of predictions to be written as

$$\hat{\mathbf{Y}} = \Phi^*(\mathbf{x}_k, 0) + \left.\frac{\partial \Phi^*}{\partial \Delta\mathbf{U}}\right|_{\Delta U=0} \Delta\mathbf{U} = \mathbf{F} + G_{PNMPC}\Delta\mathbf{U}$$

Where G_{PNMPC} is the jacobian of the Φ^* function defined in the SISO case as

$$G_{PNMPC} = \left.\begin{bmatrix} \frac{\partial \hat{y}_{k+1}}{\partial \Delta u_k} & 0 & ... & 0 \\ \frac{\partial \hat{y}_{k+2}}{\partial \Delta u_k} & \frac{\partial \hat{y}_{k+2}}{\partial \Delta u_{k+1}} & ... & 0 \\ ... & ... & ... & ... \\ \frac{\partial \hat{y}_{k+N}}{\partial \Delta u_k} & \frac{\partial \hat{y}_{k+N}}{\partial \Delta u_k} & ... & \frac{\partial \hat{y}_{k+N}}{\partial \Delta u_k} \end{bmatrix}\right|_{\mathbf{\Delta u}=[0,0,...,0]} \tag{3.1}$$

Practical procedure to obtain G_{PNMPC} and F

One of the main advantages of the PNMPC is that it can be used with any type of model if it is possible to simulate the model. This is possible through the use of a practical procedure that allows to obtain the values of the G_{PNMPC} matrix and the free responses $\mathbf{F}$ by running multiple simulations. The procedure, described bellow, is repeated at each sample time and for each system output.

1. The free response $\mathbf{F}$ is obtained by executing the model with the past inputs and outputs and with the $\mathbf{\Delta u} = \begin{bmatrix} 0 & 0 & 0 & ... & 0 \end{bmatrix}$.
2. The first column of the G_{PNMPC} matrix is obtained by first obtaining a $\mathbf{Y_P^1}$ vector by executing the model with the past inputs and outputs and with $\mathbf{\Delta u} = \begin{bmatrix} \epsilon & 0 & 0 & ... & 0 \end{bmatrix}$ where ϵ is a relatively very small value. Then $G_{PNMPC}(:, 1) = \frac{\mathbf{Y_P^1} - \mathbf{F}}{\epsilon}$
3. The other columns of G_{PNMPC} are obtained similarly by exciting a different element of $\mathbf{\Delta u}$.

This procedure allows the algorithm to be executed with arbitrarily complex models, however, it requires repeated simulations of the system every time the G_{PNMPC} matrix and the free responses are updated.

Model mismatch treatment

In [25] it is also proposed a model mismatch treatment to the PNMPC technique as depicted in figure 3.1. it considers a fixed additive correction factor $\eta(k)$ for each uncorrected system output $y_{sc}(k)$ during all the prediction horizon. This correction is calculated by filtering and integrating the prediction error of each system output defined as $e = \hat{y}(k|k-1) - y(k)$.

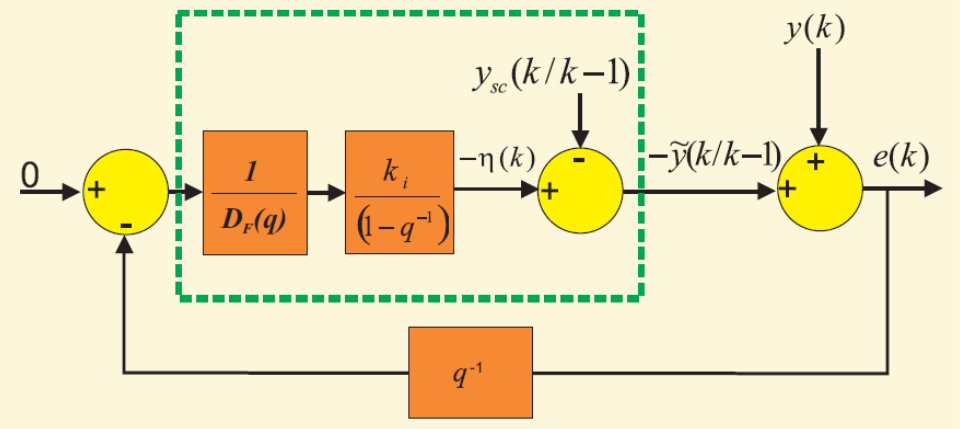

Figure 3.1: *Block diagram for model mismatch and noise treatment.*

In most cases a first-order filter in the form of $F(z) = \frac{1}{f_d z^{-1} - 1}$ is used. The same author also defines a procedure to determine the integration gain of the filter k_i and its time constant f_d to specify a critically damped response for the corrected error dynamic.

3.2 Pumping-kite optimization strategies

Contrary to wind turbines, where the trajectory of the blades (airfoils) is given by the physical constraints of the rotor, pumping-kite systems require a path optimization to maximize the energy production of the system. Overall, the path optimization is closely related to the control architecture employed and most of the previous work in this area falls in one of the two following categories: works that used decentralized control architectures, computing the kite steering and the tether's reeling speed control inputs separately, and works that employ multi variable control to jointly determine these control inputs. The groups with decentralized control strategies tend to also employ different optimization strategies for the traction and retraction phases. The off-line trajectories used in the second case are usually the product of an off-line OCP.

Much of the work in power optimization of pumping-kite systems focused on the optimal path on the fixed tether length sphere during the traction phase. However, this

path is defined mostly by the airfoil's steering command, what is not the focus of this work.

3.2.1 Off-line path generation

Following the strategy to calculate an off-line optimum solution as OCP, in [22] an OCP with closed orbit constraints, where the final state is equal to the initial state, is defined to maximize the mean power generated in a pumping-cycle considering just one eight-figure. The mean power generated is the ideal cost function as it weights not only the total energy of each phase but also how much time is spent generating and consuming energy. The problem was discretized using direct multiple shooting method, and it was used as control inputs to the kite roll angle, lift coefficient and length of tether. This solution resulted in a asymmetrical eight-shape where the final part of the path, performed close to the $\phi = 0$ plane, was used to reel-in the tether back to the initial condition.

A very similar formulation was implemented in [21]. In that work, an optimal circular orbit for a rigid wing pumping-kite system is calculated. The set of manipulated variables set is composed of the tether reeling acceleration, and the angles of the ailerons and elevator of the airfoil, that have steering and depower effects on the trajectory. To restrict control input variation, the decision variables for the optimization problem are the derivatives of the manipulated variables.

All the works presented so far are limited to off-line optimal path calculations. In [17], a closed optimal trajectory for a pumping-kite system with flexible airfoil and eight-shaped traction phase is calculated through an optimal control problem formulation. Then, it proposes a path-following NMPC combined to an estimation algorithm to follow the off-line calculated optimal path. Similarly to the previously presented works, the off-line path is calculated to maximize the average cycle power, and also like the previous works, it uses direct multiple shooting to discretize the problem and interior-point non-linear optimization to solve the created NLP.

The solution given by the OCP varies depending on the initial condition and the problem formulation. The problem described above was constructed using different coordinate systems, obtaining different results. The author speculates that the different formulations alter the solver convergence resulted in different local optima. Figure 3.2 shows the solution to the most successful formulation at different iterations of the NLP solver.

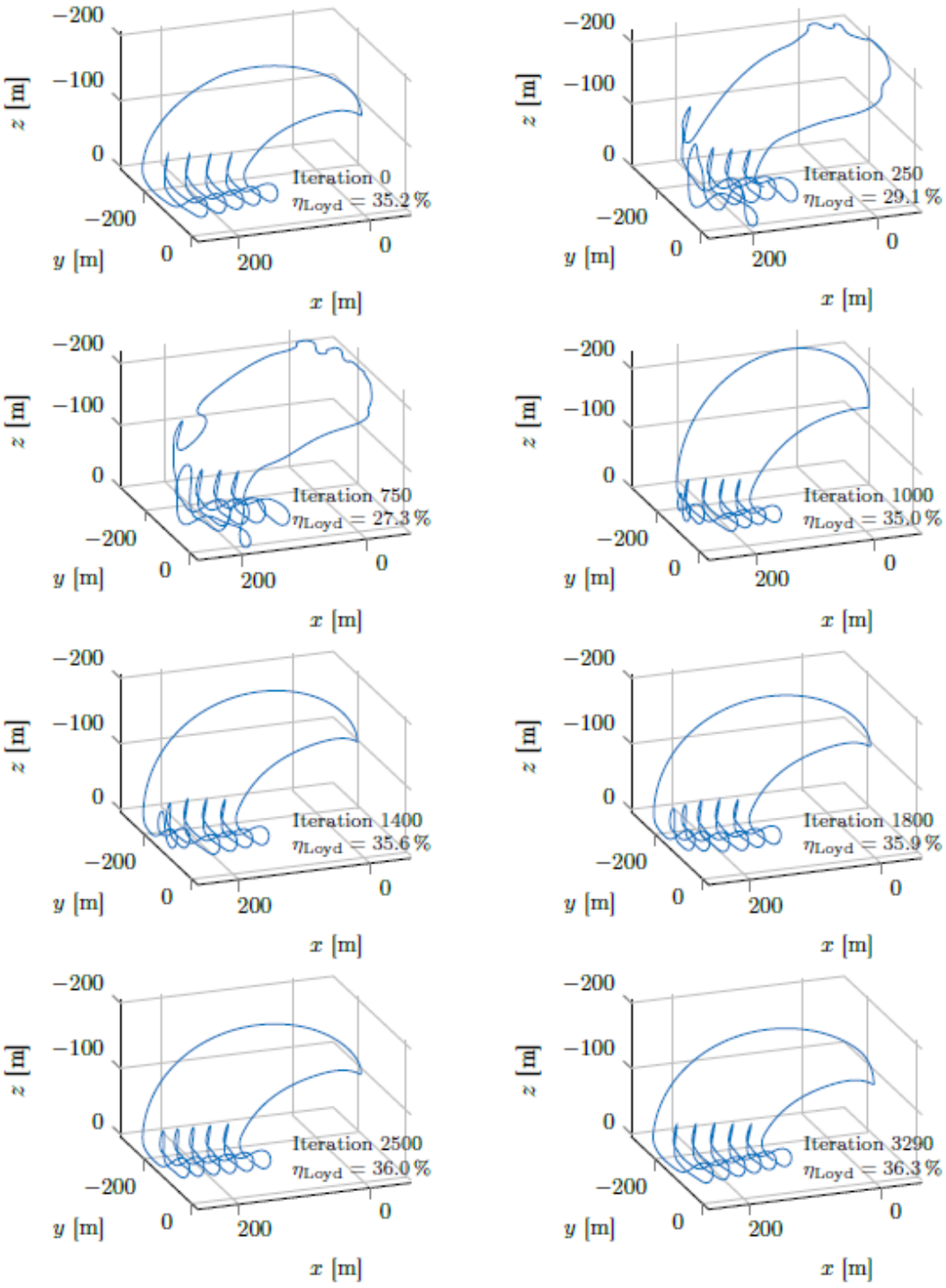

Figure 3.2: *NLP solution iteration optimizing a pumping-cycle average cycle power.*

Source: [17]

The work presented in [17] is interesting because it also considers how the optimal control can be applied and addresses some of the consequences of using an off-line generated optimal path. An off-line generated path is only optimal for the set

of parameters and wind conditions for what it was generated, however, an economical NMPC that would attempt to solve for the maximum average cycle-power trajectory is unfeasible due to the complexity of the control problem, the required prediction horizon and lack of convergence guarantees once the cost function is non-linear. To address these problems a tracking NMPC with an on-line estimator and a time warping strategy is employed. The time warping tries to adapt the optimal path calculated to the current wind condition and the on-line estimator enables a good path following even with parameter variation.

3.2.2 Traction phase optimization

While all the previously presented works are based on a closed trajectory OCP formulation other works aim to optimize different criteria in specific operation moments. These methods are usually less computationally expensive and easier to be adapted to on-line optimizations. In [32] it is argued that the off-line optimization approach leads to suboptimal results due to different wind conditions and system model errors. Besides, it is defended that the "location of the path" with respect to the wind direction is much more important than the path shape. One of the first works in this approach was [15], that used the in-equilibrium airfoil model to define traction and retraction phase by constants polar angles θ, reeling speeds $\dot{r}$, and lift and drag coefficients c_l and c_d. A single constant value could be used to describe each phase because it was assumed that the tether length variation Δr would be small compared to the optimal operation length r^*. This assumption, however, leads to very short traction and retraction phases what is undesired in practice when one accounts for the transition time between phases, when the airfoil is not in perfect traction or retraction conditions.

In [31], it is presented a reeling-out factor expression that maximizes the instantaneous power during the traction phase. The reeling-out factor is a relation of the reeling-out speed with the wind speed, resulting in the optimal value $\dot{r}^* = 1/3 sin\theta cos\phi W_n$, where W_n is the nominal wind speed at the airfoil position. In [12], a pumping cycle optimization is proposed that maximizes the average cycle power by an iterative process considering a given retraction phase strategy. This resulted in a reeling-speed 25.8% lower than the one that maximized the instantaneous power, obtaining a 9.3% increase in the cycle power. This happens because a smaller reeling-speed generates less power but during a longer period of time, therefore increasing the net power generated during the whole pumping-cycle. This result is supported by the OCP previously presented in [17]. Figure 3.2 shows the optimization iterative solution where a solution with an extra lemniscate is achieved.

It is common, in the optimization of the traction phase, to not approach the opti-

mization of the lemniscate or circle ϕ position. It is quite easy to show that the best ϕ position of flight is directly aligned to the wind speed, what in the inertial coordinate system corresponds to $\phi = 0$. Therefore, systems where the speed direction can be measured will align the center of the path trajectory with the wind direction.

3.2.3 Retraction phase optimization

In spite of being complementary to the traction phase, only a few papers have been published with the focus on the retraction phase. However, observe that it does not matter that the traction phase generates huge amounts of energy if this energy needs to be spent during the airfoil recovery. Ideally, an optimization strategy needs to consider how each phase affects each other and always aims to maximize the cycle power.

During the evolution of pumping-kite systems different retraction maneuvers were proposed. With flexible airfoils, like kites, is where the most options were discussed. According to [28] there are three maneuvers that can be used to perform a kite retraction in a pumping-kite system:

- **Wing glide maneuver**: consists of pulling the kite like a flag, with the apparent wind aligned to lateral axis of the kite.
- **Low-power maneuver**: consists of first leading the kite to the border of the wind window, that is, to a region where the wind provokes a weaker aerodynamic force, and only then rewinding the tether with a very low traction force.
- **Dive maneuver**: consists of using a continuous depower actuation to rewind the tether while it is heading to the border of the wind window.

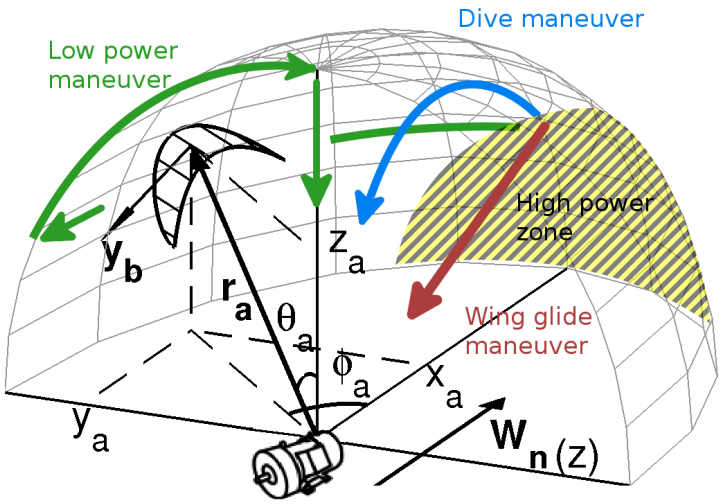

Figure 3.3: *Different retraction maneuvers present in the literature.*

Source: [28]

The first maneuver was proposed in [15] along with an optimization strategy similar to the one proposed for the traction phase, where it approximated the kite behavior during the retraction phase by the behavior in a single trajectory point. Once again this optimization strategy becomes inadequate if the tether length variation during operation is not very small. The maneuver itself also faced problems in account to the challenges to re-orient the kite after the retraction has ended.

The low-power maneuver, also proposed in [15], presents a very reliable way to retract the kite and a smaller control challenge with respect to the previous maneuver, what encourages its use in real life systems still under development. In fact, it has been successfully used in systems with no depower actuation. The main problem with this maneuver is that it takes a long period of time to complete diminishing the power generation time and consequently the cycle-power.

For being able to remedy the low-power maneuver problem while avoiding the re-orientation challenges of the wing glide maneuver, the dive maneuver is the choice of many systems. During this maneuver the kite must be guided to the border of the wind window, i.e. the kite "dives" toward the gorund station while the polar angle θ decreases, where the traction force is weaker.

In [12] a retraction optimization is presented where the optimal retraction trajectory is defined by a traction force reference trajectory and a depower actuation trajectory. For simplicity and actuation limitations both trajectories were defined as ramps with fixed coefficients so that the only decision variables were the final values of traction force and depower. This process, however, was only applied as an off-line optimization.

In [23], it is studied the influence of choosing different wind window border locations

to head to during the retraction phase with constant traction forces and the variation of the optimal traction force with the wind condition. Figure 3.5 shows the normalized cycle power for different traction forces and retraction way-points. A retraction way-point defines a (θ_R, ϕ_R) points for which the kite is headed during the retraction phase. The effect of different way-points can be seen in figure 3.4.

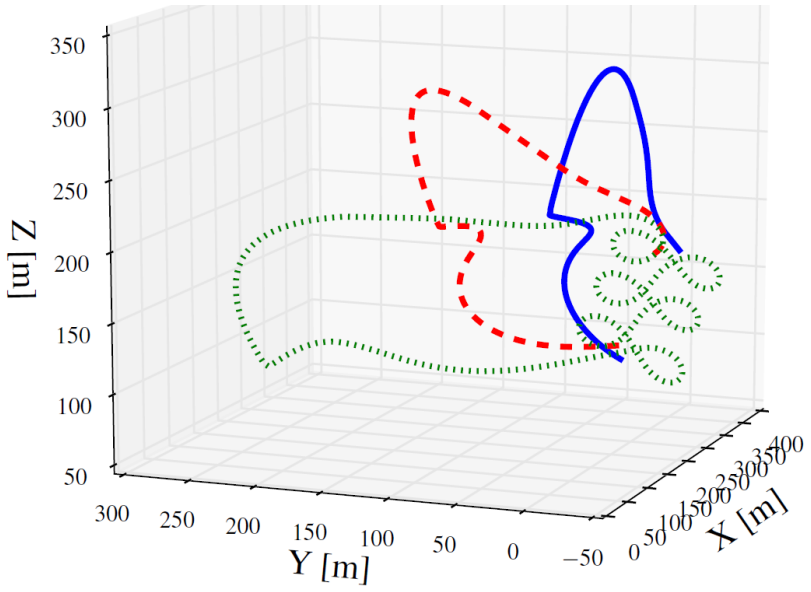

Figure 3.4: *Retraction trajectory with different way-points.*

Source: Adapted from [23]

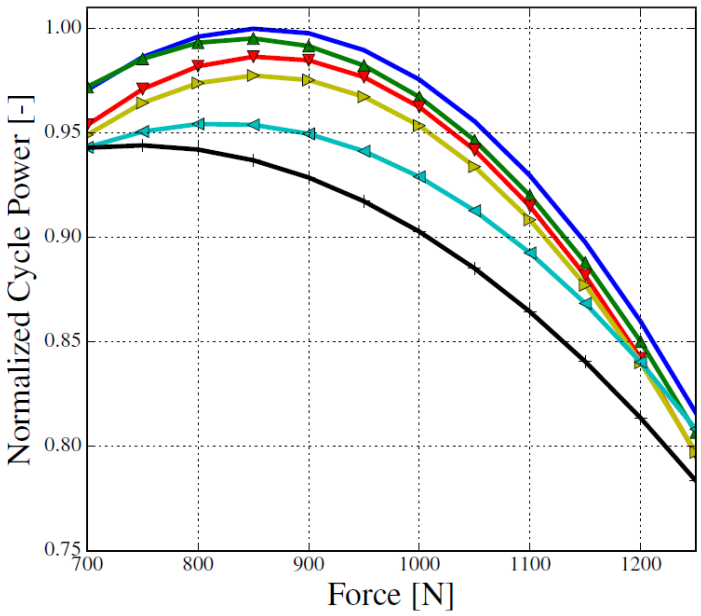

Figure 3.5: *Normalized cycle power for different retraction way points (θ_R, ϕ_R) and traction forces with a reference wind speed of 9 m/s. Dark blue curve - (90,0)^o; green - (90,30)^o; red - (90,60)^o; yellow - (90, 90)^o; light blue - (60, 90)^o; black - (30, 90)^o*

Source: Adapted from [23]

It can be observed that the optimal path for the retraction phase for most wind conditions is to move the airfoil against the wind in the $\phi = 0$ plane. The main advantage of this trajectory is that as the kite moves in the direction of the ground station it comes closer to a position where the tether goes straight up. This results in a gradually bigger gravity force in the direction of the tether, reducing even more the tether traction. In very strong wind conditions, however, the $\phi = 0$ trajectory presented a sufficiently strong apparent wind to attain the reference traction force without the need to increase the tether reel-in speed, resulting in suboptimal solutions.

The final optimization solution in [23] proposed an iterative strategy to define the retraction way-point and the final traction force in order to maximize the average cycle power considering that the traction varies from the traction phase value to the defined final traction in a ramp with fixed coefficient.

3.2.4 Phase transitions and the transition phase

The first optimization strategies just discussed did not account for the maneuver between the traction and retraction phases and vice-versa. In the closed-orbit OCP approach this was naturally accounted for and this was a strong argument in favor of the use of this approach.

More recent works have addressed this issue thoroughly, defining conditions for the beginning of each phase and pondering the time and power of these transitions. The transition from the traction to the retraction phase however, is almost seamless, once it is guaranteed that the retraction phase begins at the same point in space where the traction ends. The retraction phase, on the other hand, has its end defined only by the tether length and it frequently ends at a low θ value where the airfoil is near the zenith. To start another traction phase the airfoil needs to move to the traction phase region, what may take some seconds to happen. To work with a closed orbit with no undefined intervals this period where the airfoil moves from the end of the retraction phase to the beginning of the traction is called the transition phase.

With this in mind the full set of conditions to change from one phase to the other can be presented.

- **From traction to retraction phase:** tether length must have reached a maximum value and, to ensure a smooth transition, the airfoil must have its velocity vector as close as possible to upwards. The latter condition can be $\dot{\theta} \geq 0$ and $|\dot{\phi}| \leq \epsilon$, where ϵ is a very small value.
- **From retraction to transition phase:** The tether length must have reached a minimum value.
- **From transition to traction phase:** The airfoil must have reached a minimal polar angle $\theta \geq \theta_{min}$.

In systems where there is no transition phase, the traction phase begins at the retraction end-point. In [23] it is argued that this is undesired because a premature traction phase initiation will reel-out the tether with a smaller tether traction, resulting in a smaller power generation.

3.3 Final remarks

This chapter covered the most relevant works that affected the solution to be proposed in this work. In the nonlinear model predictive control the general two approaches were presented, providing options for the design of the solution. However, several other algorithms and techniques on the topic were not studied or discussed, characterizing a vast field of exploration for alternative works. The second section covered the different trajectory optimization options that serve as reference or as a comparison for the solution that will be proposed in the following chapter.

Chapter 4

Trajectory optimization strategy

This chapter covers the design and details of the trajectory optimization algorithms proposed for each phase of a pumping-kite system. The solutions are proposed considering the system's control architecture and the requirements that will be presented, and based on the reviewed related works.

The requirements of a trajectory optimization strategy are invariably related to the solution's optimality, its robustness to noise and uncertainties, and its performance. The first two requirements are exclusively related to the algorithm's design and do not depend on the hardware used for implementation. Performance requirements, however, are dependent on both implementation choices and algorithm design and indirectly affect the other requirements, since a limited computational time limits the optimization algorithms complexity. Moreover, a lengthier computational time limits the execution frequency of the algorithm leading to slower response to disturbances.

With all that in mind, the performance requirement was the first to be settled. Based on the system dynamics it was desired that the algorithm runs at least ten times per second, defining a target sample time of 100 ms. Considering the currently employed hardware, a 1GHz single core single board computer, that is a very ambitious target. However, this requirement does not need be directly tied to the current hardware, given that a second computation unit dedicated to the optimization algorithms could be added or the current one could be upgraded. Using the hardware as a degree of freedom relaxes this requirement, but this target value must be kept in mind as a complexity limit for the proposed solution.

To evaluate the solution's optimality is also not easy. In most cases the problem formulation seeks to guarantee that the solution is optimal based on a given criterion, but even in this case it is necessary to address the possibility of local optima, that is still a challenge in non-linear optimization. The most promising approach found in the literature is to define a closed OCP for the complete pumping cycle, however, previous solutions have only used this approach to generate off-line trajectories due to the high computational cost of non-linear optimization algorithms, lack of consistency of the solvers, and the resulting problem size on account of the pumping cycle duration, which is typically in the range of a few minutes.

Although the traction phase optimization algorithms presented have shown good

results and are light enough to be executed on-line, as done in [23], the retraction phase algorithms are still either too slow to be executed on-line or depend on the measurement of multiple pumping-cycles to converge. The reviewed works also define rigid trajectories for depower and traction force during the retraction phase. These predefined trajectories are usually based on equipment limitations and do not account for constraints in execution time, making the solutions susceptible to constraint transgressions in case of sudden strong winds or dead wind.

In summary, the ideal solution would be an economic NMPC that directly maximizes average cycle power, however, this solution is unadvised due to high problem complexity and no convergence guarantees. The tracking-NMPC solutions address the previous solution problems, however it restricts the solution to a given wind condition. Solutions specific to the traction and retraction phases are able to obtain good results, but it is harder to prove that they achieve the optimal solution in respect to cycle power, specially in the case of the retraction phase, where the existing algorithms restrict the shape of the reference signals to ramps.

The proposed solution in this work aims to combine the best of both approaches discussed. A traction phase on-line optimization algorithm is proposed, adapting the work presented in [12] to a lighter on-line algorithm. For the retraction phase, an economic PNMPC with a quadratic cost function, which avoids convergence problems, is proposed with the goal of maximizing the retraction speed while minimizing the instantaneous power spent. At last, the transition strategy adopted is revised achieving a complete pumping-cycle path planning.

The rest of this chapter will approach each phase separately and in more details. Since the retraction phase is where most of this work contributions are present it will be addressed first.

4.1 Retraction phase

Once more, the purpose of the path optimization in this phase is to define a set of traction force and depower references that lead to the most economical kite retraction, that is the one that maximizes the average electrical power generated in a pumping cycle. This formulation by itself is already implicitly limiting some aspects of the retraction phase, among which the most relevant is the steering influence on the airfoil's trajectory. The steering is removed from the optimization problem by limiting the retraction trajectory to the $\phi = 0$. In [23], a retraction on the $\phi = 0$ plane is shown to be the best solution for most cases due to the effect of the system's weight on the tether traction force. By adopting this retraction trajectory it can be assumed that steering control

system will maintain the airfoil constantly in the $\phi = 0$ and the steering dynamics can be completely removed from any models used in the optimizations.

4.1.1 Algorithm choice

The real time iteration scheme NMPC derived from general OCP formulations presented in [17] was the first algorithm considered for this work. It had already been successfully used to implement tracking-NMPC and had very good reported computational time. Besides that, the implementation of this algorithm is fairly simple through the use of the ACADO toolbox. However, the PNMPC was chosen in the end for two reasons. The first was the lack of a simple analytical model for the aerodynamic coefficients curves. The estimation of the aerodynamic coefficients curves is still under development with only an initial approximation of the shape of these curves being available. To implement a fully analytical model in ACADO it would be necessary to approximate these curves even further by polynomial approximations or by tangential planes at each sample period. It was undesired to adopt such measures without having a throughout understanding of the effect of these simplifications. The second reason for using the PNMPC was the lack of familiarity with the real time iteration scheme. The aforementioned solution is heavily derived from general OCP and NLP knowledge that is not the expertise of the author or of the UFSCKite group as a whole. By using the PNMPC, the extensive knowledge of traditional MPC theory is more easily adapted and integrated to the proposed solution, allowing this work to achieve a more robust and trustworthy implementation.

4.1.2 Cost function

By proposing a dedicated PNMPC to the retraction phase, the problem could be further broken down. The main difficulty with a PNMPC that aims to directly maximize the cycle power is that the algorithm must consider the complete retraction phase trajectory to take its decisions. Since the retraction duration is at least two orders of magnitude longer than the system's dynamic times a huge prediction horizon is required. The proposed formulation, however, aims to directly translate the instantaneous compromise that must be made at every instant of the retraction phase in the cost function, which is "is it worth spending more power to reel-in the airfoil faster?". With that in mind, the following cost function was proposed

$$J(\mathbf{\Delta u_d}, \mathbf{\Delta T}) = \sum_{j=N_1^{r_p}}^{N_2^{r_p}} \delta_{r_p}(j)[\hat{r_p}(t+j|t) - w_{r_p}(t+k)]^2 + \sum_{j=N_1^{P}}^{N_2^{P}} \delta_P(j)[\hat{P}(t+j|t) - w_P(t+k)]^2 + \sum_{j=1}^{N_u^T} \lambda_T(j)[\Delta T(t+j-1)]^2 + \sum_{j=1}^{N_u^{u_d}} \lambda_{u_d}(j)[\Delta u_d(t+j-1)]^2 \tag{4.1}$$

where the vectors of future increments of the traction force $\mathbf{\Delta T}$ and of the depower actuation $\mathbf{\Delta u_d}$ are the decision variables, the fist two summations penalize the error of the predicted tether reeling speed $\hat{r_p}$ and predicted mechanical power $\hat{P}$, to a reeling speed reference w_{r_p} and a mechanical power reference w_P, respectively. These errors are considered in two different prediction horizons defined by $N_1^{r_p}$ and $N_2^{r_p}$, and by N_1^P and N_2^P. The last two summations penalize module of the future increments of the control inputs within a control horizon defined by N_u^T and $N_u^{u_d}$. The contribution of each of these terms to the final cost is weighted by specific weights to each term. The reference errors weights are denoted by δ_{r_p} and δ_P, and the weights for the control inputs variations are denoted by λ_T and λ_{u_d}.

This is a generic MPC cost function penalizing the reeling speed and mechanical power tracking errors and the variation of the control inputs. The true purpose of the cost function is to maximize the reeling speed and minimize the power consumption. However, by writing it as a reference error it takes a more traditional form and the intended purpose still can be obtained by setting a very negative reeling speed reference, i.e. to reel-in the tether faster, and a positive or null mechanical power reference.

Definition of weights

With the proposed solution the energy and time spent during the retraction phase will depend on the weights assigned to each of these variables in the cost function, more specifically, on the ratio of $\delta_{r_p}(j)/\delta_P(j)$ at each instant. After the first results are obtained, a brief study will be conducted on the ideal ratio of the weights. The cost function formulation above assumes that the weights at each time instant can be different. Hopefully, a constant weight ratio during all the retraction phase will be sufficient to achieve a near optimal solution. More complex weight heuristics can be explored in further works.

4.1.3 Constraints

Since the constraints are an essential part to guarantee a robust flight of the airfoil it deserves a space to be discussed. In the PNMPC, the constraints are implemented as a set of linear constrains in the form of $A * \mathbf{\Delta u} = \mathbf{B}$, where $\mathbf{\Delta u}$ is the manipulated variables future increments. To ensure robust flight of the airfoil and that the physical limitations of the electrical machine are respected, the following constraints are imposed.

1. Maximum and minimum tether traction force: the maximum traction traction supported by the tether must be respected to avoid tether rupture, while a minimum tether traction force is necessary to ensure the airfoils controllability.

2. Maximum and minimum depower actuation: the depower actuation is normalized so that $0 \leq u_d \leq 1$. Besides these hard limits, sometimes it is necessary to restrict even further the depower range to avoid unstable flight.

3. Tether reeling speed saturation: given by the electric machine maximum speed.

4. Tether reeling acceleration saturation: also given by the electric machine.

5. Electric power saturation: also given by the electric machine maximum power rating. This constraint is applied to the mechanical power in practice since it is the actual predicted variable. The systems efficiency can be used to translate from one domain to the other.

6. Minimal apparent wind: a minimal apparent wind component perpendicular to the tether direction ensures the airfoil controllability. This restriction was previously used in [17] and will indirectly limit a combination of a minimal tether traction force and the depower actuation, making the minimal traction force constraint redundant. In this work the minimal apparent wind component was calculated as $W_a^\tau = (sin\theta * W_n - \dot{r})) * E$.

Constraints1 and 2 limit the manipulated variables, therefore the controller can guarantee that they will be feasible. The remaining ones, however, can only be exerted upon the predicted value of the outputs that are calculated from the linearized model at the current sample time. Therefore, the future predicted mechanical power vector $\mathbf{P}$, for example, would be calculated as $\mathbf{P} = G^P_{PNMPC} * \mathbf{\Delta u} + f^P$, where f^P is the free response of the system's mechanical power.

Also note that, besides the mechanical power and the tether speed the constraint set creates the need to linearize and calculate the minimal apparent wind. This leads to an extra system output that does not appear in the cost function.

Soft constraints

Since the output constraints are subject to model and linearization errors, they often result in impossible formulations for the quadratic optimization problem. This happens, for example, when a controlled variable briefly disrespects a max/min constraint and cannot return to the allowed region in one sample time.

To avoid optimization problems with no solution during the system operation, a constraint relaxation technique was used which consists in adding a constraint error decision variable ϵ to all controlled variables constraints. For example, a maximum power constraint $\mathbf{P} \leq \mathbf{P_{max}}$ would become $\mathbf{P} \leq \mathbf{P_{max}} + \epsilon$. To ensure that all ϵ will remain as close as possible to zero an extra term is added to the optimization cost function with very high weight.

4.1.4 Model mismatch treatment

The model mismatch treatment proposed by [25] for the PNMPC is also applied to guarantee that the output restrictions will be respected in steady-state regimen. It is possible that the treatment would not be necessary due to the estimation algorithms employed in the system, however, by adding the correction the solution becomes more general and self sustainable.

The main sources of prediction error will probably lie in the aerodynamic coefficients estimation and in the variations of the wind. Since a wind gust model is not employed in the internal model, only the average nominal wind speed is taken into consideration. The incorporation of a wind gust model or the use of stochastic control algorithms to deal with the wind unpredictability can be subjects of future works.

The model mismatch treatment is applied to each output model free response considering that the error will remain constant during the entire prediction horizon, as proposed in the original work where. The correction is calculated by integrating and filtering each output's prediction error.

4.1.5 System model and problem formulation

The system model was not addressed so far in this chapter because it does not change the PNMPC algorithm procedure and is even less important when the free response and the G_{PNMPC} matrices are being calculated through simulation, which is the case for this work. However, it is imperative that, in future works, a less time consuming alternative is implemented to achieve a better performance.

The internal model used for the PNMPC is the point-mass model presented in section 2.2.3. One important modification to the formulation presented is the addition of the traction force control dynamics. The addition of the traction force controller inserts extra dynamics to the system, with an additional state space variable given by the traction force itself, which was previously treated directly as a manipulated variable. The traction force reference replaces it as a manipulated variable and the following dynamic equation is added to the model that assigns a fixed error dynamic to the traction error.

$$\dot{T} = \frac{(u_T - T)k_{tr}J_L}{r_d}, \tag{4.2}$$

where u_T is the traction force reference, k_{tr} is the gear box transmission gain, r_d is the system's drum radius, and J_L is the system's moment of inertia.

With all the essential parts of the controller defined, the whole retraction phase pseudo-code can be stated.

Algorithm 1 Retraction phase procedure

```
1: procedure Retraction phase
2: loop:
3:     Update measurements
4:     if r ≤ r_min then
5:         goto Transition Phase.
6:     Calculate free responses and G_PNMPC matrices
7:     Construct QP problem
8:     Solve for traction force and depower increments
9:     Increment and apply controls
```

4.2 Traction phase

The traction phase optimization algorithm developed here is heavily based on the optimization presented in [12]. First, the traction phase optimization problem will be reviewed, then, later, the solution proposed will be presented.

As a specification from the steering control system, it is assumed in this work that the lemniscate will be the airfoil's trajectory during the traction phase. The airfoil's lemniscate trajectory, more specifically, the lemniscate of Bernoulli, could be parameterized by the distance of its focci, and the (ϕ_l, θ_l) coordinates of its center. However, since the optimal ϕ_l position of the trajectory is trivially obtained as $\phi_l = 0$, the optimal trajectory parameters to be defined during the traction phase are only the lemniscate's elevation θ_l^* and the focus a_f. Although in many previous works these parameters are considered to be constant during the whole trajectory, a more general and optimal solu-

tion would consider them to be time variant or, at least, dependent on the tether length. The optimal trajectories found in works that employ closed orbit OCP are a good reference to evaluate the importance of varying the lemniscate elevation and its focuses during the traction phase. In [17], by specifying a minimal height constraint instead of a maximum θ for the airfoil's trajectory a 2.1% larger cycle power efficiency was obtained, indicating that a varying lemniscate elevation during the traction phase can be beneficial. No similar results were found to the variation of the lemniscate's focus coordinate, instead, by qualitatively comparing the OCP results, that have no constraint in the ϕ coordinate, it is observed that the airfoil's movement tend to broaden as the tether length increases, suggesting that a fixed lemniscate focus a is a good approximation.

Besides the airfoil's trajectory, the optimal traction phase is also defined by the optimal tether reeling-out speed $\dot{r}^*$, variant during the phase, the optimal tether length r^* and the optimal tether variation Δr^* around r^*.

In summary, in a discrete time system the most general traction phase trajectory could be defined by: the lemniscate focus vector **a**, the lemniscate polar angle vector θ_1^*, the tether reeling-out speed vector $\dot{\mathbf{r}}^*$, the optimal tether length r^* and the tether variation Δr^*.

4.2.1 Modifications to on-line optimization

In [12] an iterative algorithm is proposed to define the optimal tether length r^*, the optimal constant tether reeling-out speed $\dot{r}^*$, the optimal angle of attack α^* and the optimal constant lemniscate polar angle θ_l^* for the traction phase but optimizes, at the same time, the retraction phase. In an effort to adapt the iterative algorithm to an on-line optimization, the time and energy spent in the retraction phase can be obtained from the last cycle's retraction phase instead of the retraction phase optimization, enabling the definition of an non-iterative optimization problem that maximizes the average cycle power and computes the r^*, $\dot{r}^*$, α^* and θ_l^* set. The optimal angle of attack does not need to be optimized for this work since a foil kite with fixed base angle of attack is used, however, the equilibrium angle of attack needs to be determined to properly calculate the traction force. This calculation can be incorporated in the optimization problem by defining the angle of attack as a decision variable and using equality constraints to ensure the equilibrium condition.

It is very challenging to determine an optimal tether length variation, without accounting in detail for the effect of the transition and retraction phases, what is very hard to incorporate in a sufficiently fast optimization algorithm. As an example, the iterative optimization procedure proposed in [12] took more than one minute to complete. For this reason, it was decided to adopt a fixed relative tether length variation where the

tether variation is defined as a fraction of the optimal tether length,

$$\Delta r^* = c_{tv} r^*$$

where c_{tv} is the tether variation coefficient. The optimal tether variation coefficient can be studied off-line to obtain better results. If the tether variation coefficient is too big, the airfoil will operate too far from the optimal tether length. On the other hand, a too short coefficient will be more affected by the transition phase time. A larger tether variation also has an impact on the retraction phase's end position since it implies a longer retraction phase resulting in a lower end polar angle θ.

As a final adaptation to an on-line algorithm, it is proposed to make a two step optimization: a first optimization in a slower frequency to define r^*, and consequently, Δr^*, and another, in a faster frequency to define $\dot{r}^*$ and θ_l^* based on the current tether length, thus enabling the algorithm to provide a different optimal tether speed and elevation angle at each moment of the retraction.

With the proposed modifications, many of the general trajectory parameters are optimized, with the exception of the lemniscate focus and tether variation, being the former approximated by a constant, off-line calculated value, whereas the later is approximated by a fixed relation with the optimal tether length that can also be optimized off-line.

Reeling speed control

Apart from the optimization procedure described so far it is also necessary to control the reeling speed to match the optimal reeling speed calculated by manipulating the tether traction. The reeling speed control proposed is shown in figure 4.1. During the average power optimization, the tether traction reference T_{ref} that corresponds to the optimal reeling speed $\dot{r}^*$ will be calculated. However, the algorithm's internal model may contain errors with respect to the real system, leading to a different reeling speed after the traction control loop stabilizes.

This work proposes the use of a similar model mismatch treatment applied to the retraction phase to correct the reeling speed error in the traction phase. Figure 4.1 shows the proposed treatment, containing a similar first order filter and an integrator with a integration gain k_i, added to the simplified control traction loop.

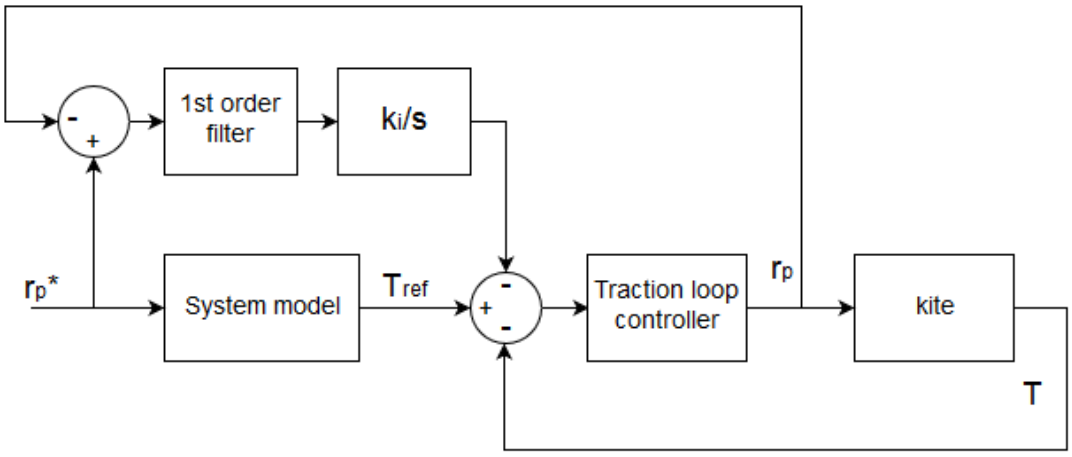

Figure 4.1: *Block diagram illustrating the correction treatment integration to the traction control loop.*

Source: Original

One may rightfully question if the model mismatch treatment proposed interferes with traction loop controller. Indeed, if not carefully designed, the addition of the treatment may yield unexpected results. To avoid this problem, the dynamics of the optimal reeling speed error must be much slower than the traction control loop dynamics, separating, therefore, the two controllers in different frequency regions. The longer convergence time of the reeling speed error does not present a problem for the system's operation as the traction force controller already addresses the problem of wind gusts and the optimal reeling speed should not vary a lot during the traction phase.

4.2.2 Optimization equations and constraints

Due to the relative simplicity of the model used, the complete non-linear optimization problems constructed can be shown here.

Operation point optimization

The optimization problem that defines the optimal tether length and its variation will be addressed, henceforth, as the operation point optimization.

Unfortunately, The definition of the optimal polar angle and the optimal tether reeling speed at the optimal operation point is not trivial and must be jointly computed in the optimization problem. For this reason, the complete set of variables, including tether speed, polar angle, and angle of attack is computed aiming to maximize the cycle power.

The cycle power is calculated by approximating the traction phase's total generated energy by the optimal instantaneous power times the phase duration. Since we are treating the transition phase as a separate phase, its time and energy also needs to be accounted for in the cycle power:

$$P_{cyc} = \frac{P_{trac}\Delta t_{trac} + P_{ret}\Delta t_{ret} + P_{trns}\Delta t_{trns}}{\Delta t_{trac} + \Delta t_{ret} + \Delta t_{trns}}$$

where P denotes average power and Δt the total phase time. The subscripts $trac$, ret, and $trns$ reference the traction, retraction and transition phases, respectively.

The average powers and phase times of the retraction and transition phases are approximated by the values of the last retraction and transition phases. The average power of the traction phase is given by the instantaneous maximum power $P^* = T(\alpha, \theta_l^*, r^*, \dot{r}^*)\dot{r}^*$, where T is the traction force at the optimum point given by equation 2.20. The total traction phase time is approximated by a constant tether reeling speed through the entire $\Delta t_{trac} = \frac{\Delta r^*}{\dot{r}^*} = \frac{c_{tv} r^*}{\dot{r}^*}$ length. The cycle power thus becomes

$$P_{cyc} = \frac{T(\alpha, \theta_l^*, r^*, \dot{r}^*)c_{tv} r^* + P_{ret}\Delta t_{ret} + P_{trns}\Delta t_{trns}}{\frac{c_{tv} r^*}{\dot{r}^*} + \Delta t_{ret} + \Delta t_{trns}}$$

Besides the model equations and the cost function, the optimization process also needs to incorporate the problem's constraints. The complete set of constraints for the operation point optimization are:

1. Maximum tether traction force;
2. Minimum lemniscate elevation angle;
3. Maximum tether reeling speed;
4. Maximum and minimum optimal tether length;
5. Electric machine's power saturation;
6. Minimum airfoil altitude;
7. Equality constraint to define α;

Finally, the complete optimization problem is presented

$$\underset{r^*,\theta_l^*,\dot{r}^*,\alpha}{\text{minimize}} \quad P_{cyc}(r^*, \theta_l^*, \dot{r}^*, \alpha)$$

subject to

$$\begin{aligned}
&(r^*, \theta_l^*, \dot{r}^*, \alpha) \leq u_{UB} \\
&-(r^*, \theta_l^*, \dot{r}^*, \alpha) \leq -u_{LB} \\
&T(\alpha, \theta_l^*, r^*, \dot{r}^*) - T_{max} \leq 0 \\
&\dot{r}^* T(\alpha, \theta_l^*, r^*, \dot{r}^*) - P_{max} \leq 0 \\
&r^* \cos\theta - h_{max} \leq 0 \\
&c_l * sin(\alpha) - c_d * cos(\alpha) = 0
\end{aligned}$$

where h_max is the maximum altitude and the last constraint corresponds to the equality constraint used to define α and is obtained by the the cancellation of forces on the tangent plane. This expression also considers that the set of aerodynamic forces are much stronger than the set of remaining forces, disregarding the later set.

Tether reeling speed and lemniscate elevation optimization

The second optimization problem defined, that optimizes the tether reeling speed and the lemniscate elevation for the current tether length, follows the same constraint and cost function of the operation point optimization. However, in this problem the optimal tether length is not a decision variable since the tether length considered is the measured current tether length.

4.2.3 Complete traction phase procedure

The complete traction phase procedure is shown bellow

Algorithm 2 Traction phase procedure

1: **procedure** Traction phase
2: *loop*:
3: *Update measurements*
4: **if** $r > (1 + \frac{c_{tv}}{2})r^*$ and $\dot{\theta} < 0$ and $-\epsilon < \dot{\phi} < \epsilon$ **then**
5: **goto** Retraction phase.
6: $r^* \leftarrow opertaion\_point\_optimization()$.
7: $(\dot{r}^*, \theta_l^*) \leftarrow speed\_and\_theta\_optimization()$

The two separate optimizations can also be executed at different frequencies, since the result of operation point optimization is expected to change far more slowly than the reeling speed and polar angle optimization.

4.3 Transition phase

The general procedure during the transition phase is well defined: to maneuver the airfoil as fast as possible to the traction phase start region.

Reviewing the transition maneuvers adopted by other groups, a simple, yet complete, transition phase is proposed in the following steps:

1. After the end of the retraction phase, set the tether reeling speed and depower actuation directly to zero respecting the corresponding variation saturations;
2. Also, set the steering controller to follow the traction phase path;
3. When the airfoil's polar angle is bigger than a threshold polar angle, or when the tether traction force reaches a maximum threshold, the transition phase ends, and the tether begins to reel-out.

This simplified transition procedure addresses the following concerns: it guarantees that the tether traction force stays in acceptable limits, and it avoids a high speed dive towards the ground.

The addition of the maximum traction force as an alternative condition to end the transition phase may result in the traction phase beginning earlier, while the airfoil is not yet on the optimal position. However, the tether traction force surpassing the threshold is already a good indicator that a decent power generation can be achieved, even if not in the optimal position.

The choice to start following the traction phase's path during the transition may result in a slightly longer transition phase but avoids the risky maneuver of diving the airfoil directly into the ground since the traction phase trajectory will point it to the side at the same time.

Chapter 5

Implementation and Results

The trajectory optimization algorithm presented in chapter 4 was implemented in MATLAB in order to allow for integration with a simulation model of a pumping-kite AWES and to facilitate the tuning of the several parameters available.

This chapter's first section focuses on the implementation and results of the algorithm employed for the retraction phase of the pumping cycle. Since this phase takes place entirely on the $\phi = 0$ plane, a simplified simulation model without steering dynamics, as described in section 2.2.3, was utilized. Besides allowing for the retraction optimization algorithm to be tested in more stable conditions, which does not jeopardize the validity of the simulation, this approach also reduces the time needed to simulate a full retraction.

The second section, on the other hand, covers the implementation and results obtained with the algorithm employed for the traction phase. Note that although a simpler model obtained for the dynamic equilibrium situation defines the optimization problem, the full three-dimensional point-mass model was used for the purpose of validation. Except for some minor modifications, both the simulation environment and the steering controllers were taken from a previous work.

In order to compare the results with other trajectory optimization algorithms proposed in the literature, a well- defined metric is necessary. If all parameters and environment conditions used in other works were accurately reproduced, then the cycle power itself could be used as a comparison criterion, given that it is the measurement being optimized. To abstract away the effects of the wind conditions and of the characteristics specific to each AWE system, the Loyd factor η_{Loyd} is used. This quantity is given by

$$\eta_{Loyd} = \frac{P_{cyc}}{P_{Loyd}}$$

with

$$P_{Loyd} = \frac{2}{27}\rho A W_n^3 c_l E^2,$$

which expresses the relationship between the cycle power and the Lloyd theoretical power limit P_{Loyd} for a pumping-kite system.

The full set of values used to parameterize the simulation models are presented in table 5.1.

Table 5.1: *Nominal system parameters*

Parameter	**Value (unit)**
Air density	1.2kg/m^3
Gravity acceleration	9.82m/s^2
Airfoil's plus control pod's mass	7kg
Airfoil's projected area	12m^2
Airfoil's aspect ratio	5
Airfoil's fixed base angle of attack	6.8º
Tether's density	970 kg/m^3
Tether's drag coefficient	1.2
Tether's diameter	0.005m
Number of tethers from control pod to ground station	1
Electric machine's moment of inertia	0.25 kg.m^2
Drum's moment of inertia	0.1 kg.m^2
Drum radius	0.2m
Reference wind speed	7m/s
Reference wind measured altitude	15m
Surface roughness	0.05m

5.1 Retraction phase

To evaluate how the implemented solution impacts the cycle power without simulating the whole pumping-cycle, an approximation of the duration and average power of the traction phase was used.

In a first simulation scenario, the system was simulated with the exact same model used in the PNMPC algorithm, eliminating the influence of model mismatch and allowing for a more objective comparison with other solutions. This close-to-ideal scenario also facilitates the job of finding an initial good set of multiple controller parameters that affect the solution, namely the cost function's weights, the horizons sizes and the value of the different restrictions.

The results shown in figure 5.1 were obtained using a reeling speed reference of $-40m/s$ and mechanical power reference of $0KW$, and the following set of normalized weights:

$$\lambda_{r_p} = 14$$
$$\lambda_P = 1$$
$$\delta_T = 0.02$$
$$\delta_{u_d} = 0.02$$
$$\delta_{ksi} = 1000$$

The weights were normalized by dividing them by the corresponding variable saturation and the length of the prediction or control horizon. By doing this, the magnitude of the variables will not affect the cost function. Additionally, the length of the horizons used were

$$N_{r_p} = 5$$
$$N_P = 5$$
$$Nu_T = 3$$
$$Nu_{u_d} = 3$$

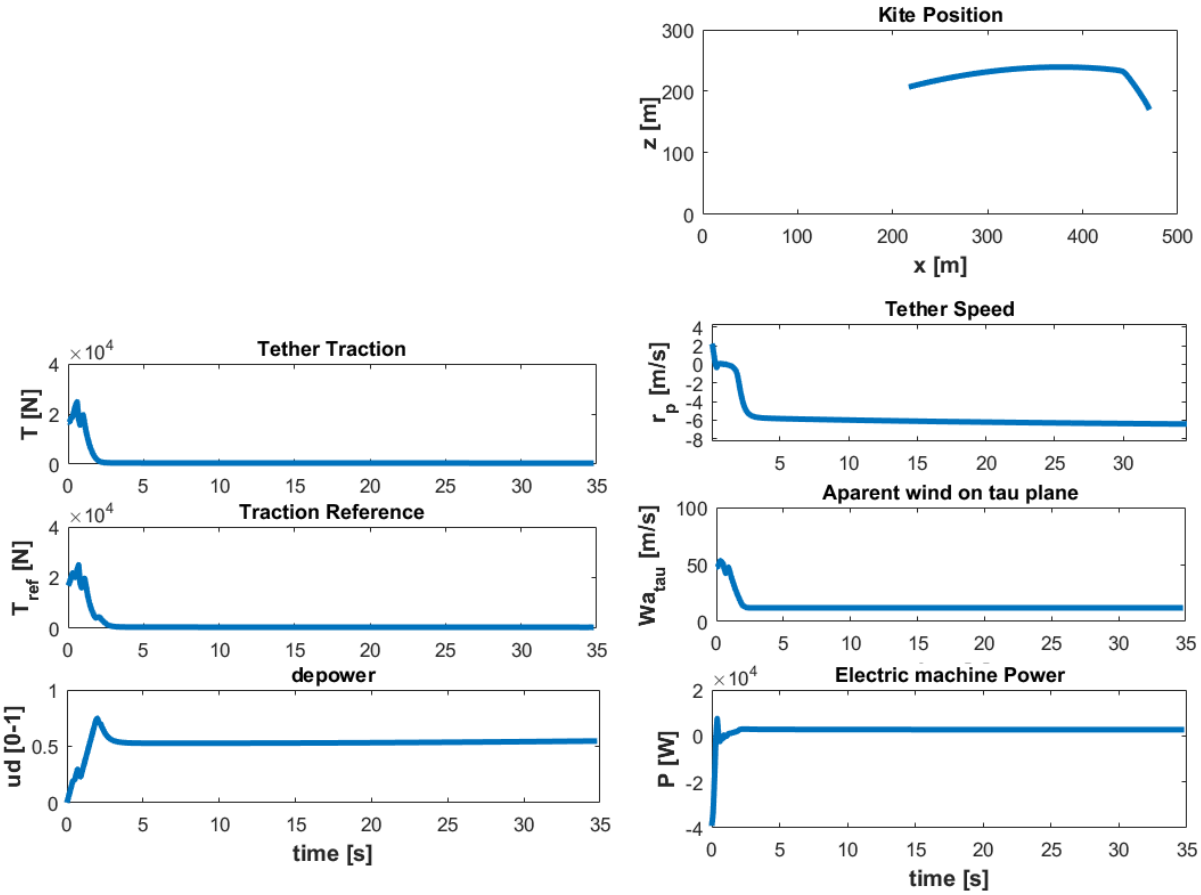

Figure 5.1: *Results for the retraction phase with nominal model parameters and wind condition.*

It can be seen that the obtained result is mainly defined by the set of constraints which was already the case for the ramp solutions previously used. However, this solution, differently from the ramps, allows for a more extensive use of the depower actuation that presents a peak to first decelerate the airfoil and reduce the tether traction force to later stabilize it in a value that respects the minimal apparent wind imposed. Another interesting effect observed is that the tether reeling speed stabilizes at zero while the kite has not fully decelerated. When using tether traction ramps, the tether is still reeled out for a brief period at the beginning of the retraction, producing a suboptimal amount of power since the kite is moving out of the high power zone. This effect has the drawback of adding an extra length of tether to be reeled in, which represents a waste of both time and energy.

The full set of restriction values used is presented in table 5.2.

Table 5.2: *Problem constraints*

Constraint	**Value**
Tether traction force saturations	300 - 80000 N
Tether traction force variation saturation	$\pm$50000 N/s
Depower actuation saturations	0 - 1
Depower actuation variation saturation	0.5 un./s
Tether reeling speed saturations	$\pm$7 m/s
Tether reeling acceleration saturations	$\pm$ 9.82 m/s^2
Electric power saturations	$\pm$100000 W
Minimal apparent frontal wind	970 kg/m^3

It is important to highlight that the actual cycle power obtained and the overall characteristics of the curves are directly related to the set of constraints employed, the weights, and the cost function itself. The algorithm presented generates tether traction force and depower actuation references that are not limited to ramps. In addition, the results show the potential of using an heuristic economic NMPC to approximate the optimal retraction trajectory, which allows for the application of an on-line algorithm with a generic and flexible set of constraints.

Since the controller is actually weighing the instantaneous power and the current speed, very short prediction horizons are necessary to obtain good results. In fact, even with single sample prediction horizons a satisfactory result is obtained. This suggests that a real-time implementation of this technique is far simpler than other NMPC based algorithms previously proposed for trajectory generation.

5.1.1 Optimal weight for different wind conditions

A pumping-kite system like other power generating systems, is designed for a nominal condition, in this case, for a nominal wind speed. When deployed in real sites, however, diverse wind conditions are encountered, demanding good performance in different scenarios.

The set of weights identified for the nominal wind condition may not be appropriate to different wind conditions. In an attempt to overcome this disadvantage and aiming at providing a more general and flexible solution, a brief study was performed in search of a weight heuristic that provides a near optimal solution to different wind conditions.

This study focused on finding the optimal ratio between the weights of the tether reeling speed and mechanical power reference errors for different wind speeds, increasing the importance given by the controller to the retraction speed with respect to that given to power consumption. To achieve this, the system was simulated with different reference wind speeds W_r and different weight ratios. Figure 5.2 shows how the average cycle power, and the Loyd factor changes for each wind condition with the variation of the weights.

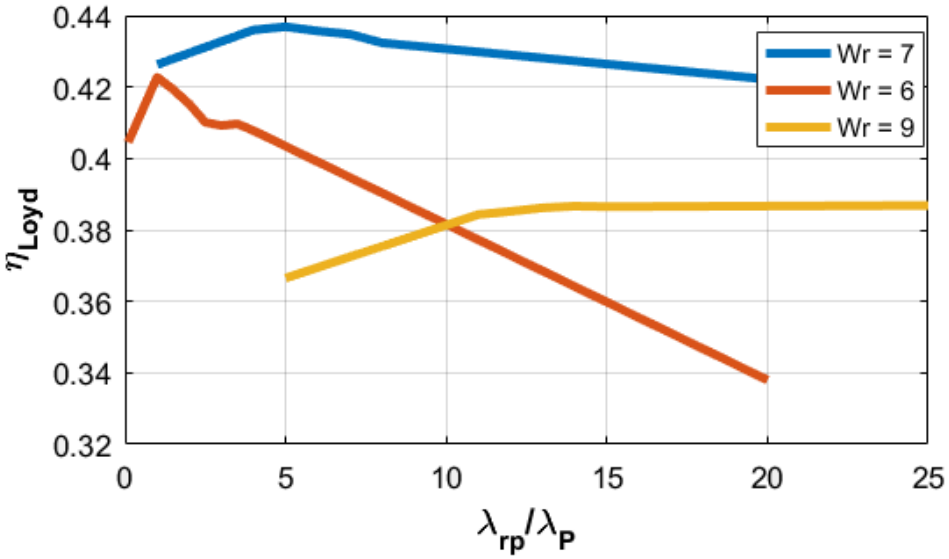

Figure 5.2: *Loyd factor η_{Loyd} for different cost function weights and for different wind conditions.*

Source: Original

The precise effect of the variation of the weight ratio is hard to understand because the weights themselves do not completely define the trajectory. However, two important characteristics were found to have a close relation to the weights.

When varying the weight ratio, the final reeling speed at which most of the tether is reeled-in changes. By increasing the weight of the reeling speed error, the tether may

be reeled at a faster speed, resulting in a shorter retraction phase, but with more power required from the electric machine. This effect was consistently observed, and contrary to initial intuition, the fastest possible reeling speed is not the most advantageous as can be seen for the scenarios of $w_r = 6$ and $w_r = 7$ in figure 5.2.

A second important characteristic of the generated trajectories is the moment at which the tether begins to be reeled in. The less significant the reeling speed error is, the smaller the polar angle at which the tether starts to be reeled in. In this condition, the airfoil is at a higher altitude but the wind direction allows for a faster retraction with lower tether traction force. These two factors explain the local optima observed for the three different wind conditions considered. An unexpected effect observed is that the Loyd factor decreases with very high wind speeds, e.g. from $w_r = 7$ to $w_r = 9$. This happens because a higher amount of energy is necessary to reel-in the tether with stronger winds.

Finally, by observing the approximated local optima in these different measured wind conditions, a heuristic is proposed that defines the weights ratio as a function of the measured wind speed. A simple, yet good, approximation observed was to define

$$\lambda_{r_p}/\lambda_P = 0.8 * W_r$$

This heuristic may not be the best way to define this relation once the optimal solution would also depend on the surface roughness and the measured wind altitude, for example, being valid only for a specific system and site. However, the procedure could be repeated for each specific case and already achieves a close to optimal average cycle power to a variety of wind conditions.

5.1.2 Model mismatch treatment

Another important component to achieve a robust flight operation is a well calibrated and functional model mismatch treatment. The main purpose of the treatment is to avoid that constraints on the output variables are not unknowingly disrespected.

Many of the system parameters are constructive and well known and therefore do not have a significant error in practice. The factors that cause the most significant errors are the measurements and estimations errors on the state variables, that is, the position and speed of the kite, and errors on the aerodynamic coefficients. It is reasonable to consider the errors on the system state as measurement noise with zero mean, therefore it shall not cause a steady-state error on the outputs. The aerodynamic force coefficients, however, are not yet well studied and it is possible that the estimated values have a significant steady state error. In this chapter, a constant multiplicative

error to the aerodynamic coefficients is considered, which affects the aerodynamic forces and, consequently, all output variables.

Figures 5.3 and 5.4 compare the outputs of the optimizer when the model's aerodynamic coefficients are subject to a 20% multiplicative error. The errors were combined to also result in a bigger efficiency error, by combining a 20% increase in drag a 20% decrease in lift and vice versa. Keep in mind that the actual nominal model and wind conditions are the same for all three results presented in figures 5.3 and 5.4.

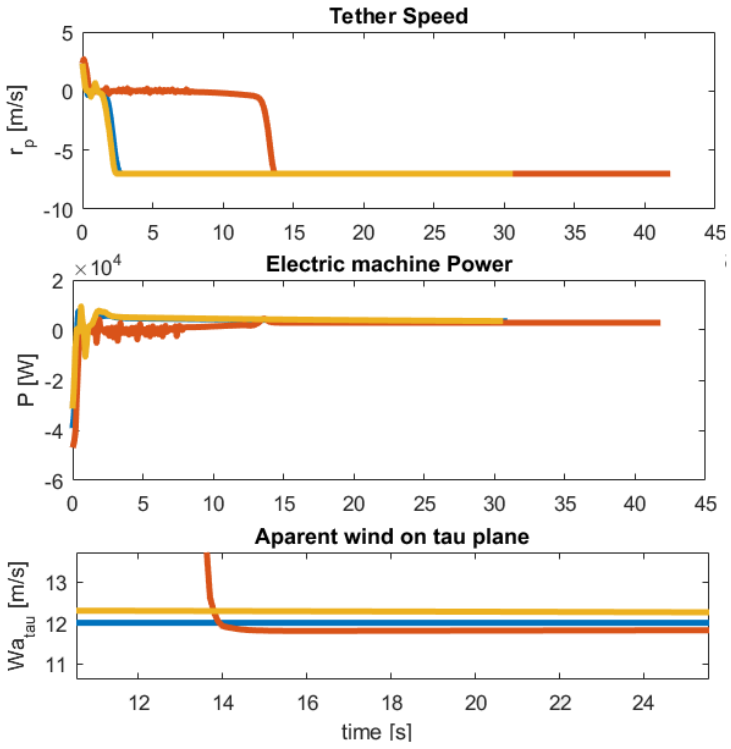

Figure 5.3: *System outputs in presence of a constant multiplicative error to the aerodynamic coefficients and with no model mismatch treatment. Blue line - no mismatch; orange line - reduced efficiency in internal model; yellow line - increased efficiency in the internal model.*

Source: Original

In figure 5.3, significant errors can be observed in all three variables. Besides the expected difference in the final apparent wind and the electric machine power, the model error also affected the moment when the tether begins to be reeled-in.

In the presence of the model mismatch treatment, however, all outputs converge to a same final value respecting the correspondent constraints. Before this final value is reached, the constant changes on the system do not allow for the model mismatch correction to fully stabilize, consequently, it is very hard to assure that the constraints imposed on the variation of the outputs will be perfectly respected.

To obtain the presented results the model mismatch treatment filter was calculated

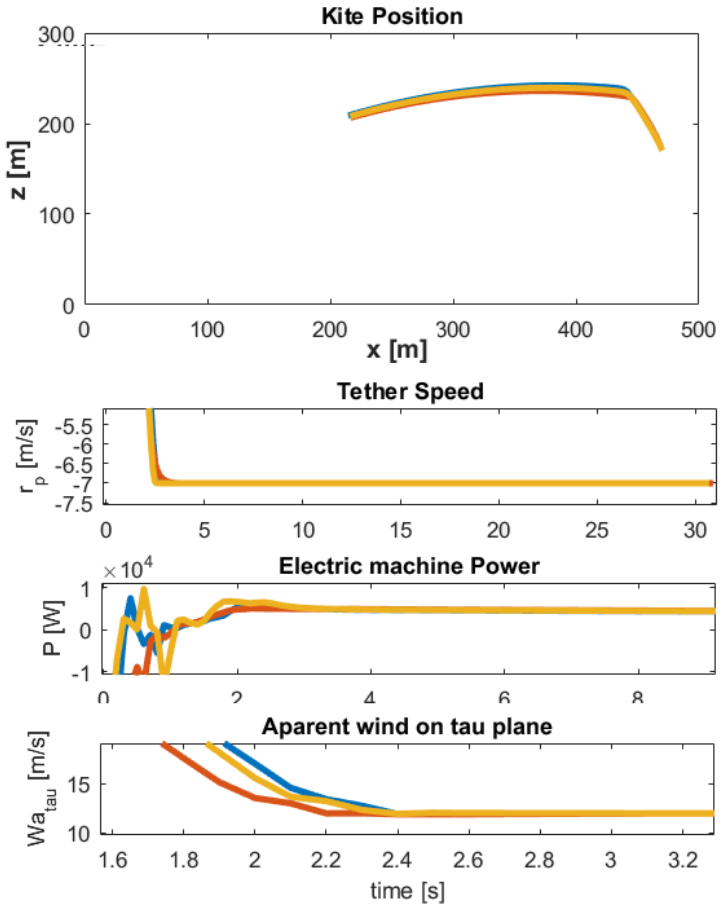

Figure 5.4: *System outputs and airfoil's position in presence of a constant multiplicative error to the aerodynamic coefficients with model mismatch treatment. Blue line - no mismatch; orange line - reduced efficiency in internal model; yellow line - increased efficiency in the internal model.*

Source: Original

to achieve a critically damped model error response with a double pole on 0.4, with a sample period of 0.1s. This is a fairly fast response. To achieve a more robust system under the presence of disturbances it may be necessary to design a filter that leads to a slower error dynamic. The designed filter had a single pole on 0.16 and a integration gain of 0.36.

5.2 Traction phase

As previously mentioned, the traction phase trajectory optimization algorithm, designed in chapter 4, was integrated to a simulation with a three dimensional pumping kite model and a steering control system proposed by [12] with a lemniscate trajectory.

To better observe the effect of the proposed solution, the optimal reeling speed is directly imposed to the system instead of being indirectly set trough the traction force

control. The optimal reeling speed calculated by the algorithm, that considers the airfoil at a $\phi = 0$ position, was used to calculate the optimal speed at different positions of the lemniscate trajectory according to $\dot{r} = \dot{r}^* cos(\phi)$. This relation does not take into account the trajectory's variations in θ, whose amplitudes are much smaller than the variations in ϕ. However, for a more general solution, the algorithm could be adapted to determine, instead of the optimal reeling speed, an optimal reeling coefficient κ that determines the reeling speed as $\dot{r} = W_n \kappa sin(\theta) cos(\phi)$, which would present less variations throughout the trajectory and would account for θ, ϕ and W_n variations without executing the optimization again.

The simulations performed represent a pumping-kite system's traction phase in which a total of 200m of tether length is released. The main points to be observed in these simulations are:

- Verify whether approximating the cycle power with the previous retraction phase energy spent and time can provide good results. In this case, the data from the previous retraction phase will be used.
- Verify the effects of running the reeling speed and elevation angle optimization multiple times during the traction phase.
- Provide a first notion of the computational cost of such optimizations.

The obtained results are presented in figures 5.5, 5.6 and 5.7. In figure 5.5 the complete airfoil trajectory can be seen. It is noticeable that a relatively low reeling speed is being employed and that there is no significant variation in the elevation angle nor in the reeling speed throughout the trajectory. By further examining these variables it is clear that, in fact, no variation occurs to the optimal elevation angle calculated, however, the optimal reeling speed r_p^* increases as the nominal wind speed increases due to the higher operation altitude.

The values for reeling speed obtained approximately match the results obtained with the full cycle optimization in [12], where it was observed that the optimal reeling speed considering the cycle power was 25.8% lower than the value that maximizes the instantaneous power. That alone resulted in a 9.3% increase in the cycle power. In this work, the reeling speed found was in average 22.24% lower than the value that maximizes the instantaneous power. This shows that the approximation of the retraction phase duration and consumed energy can be used to obtain much faster results for an cycle power optimization without significant difference in the results. The increase in the reeling-out speed as the nominal wind at the airfoil altitude increases is also very relevant but similar results could be obtained without the need to frequently execute the optimization by using a fixed reeling coefficient κ.

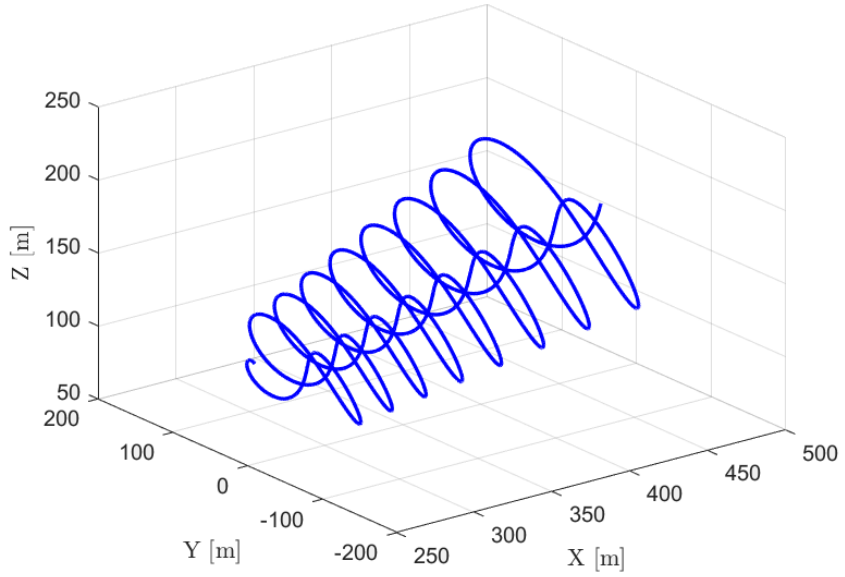

Figure 5.5: *Three dimensional airfoil trajectory during the simulation.*

Source: Original

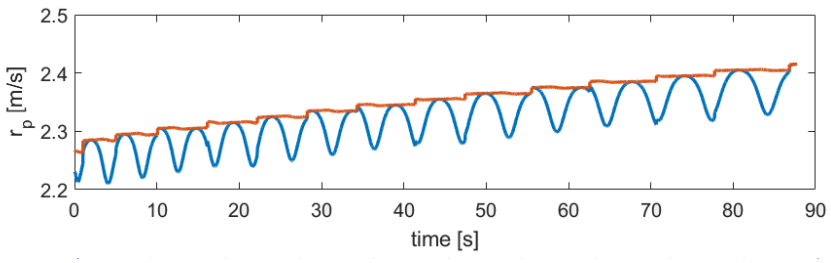

Figure 5.6: *Tether reeling speed with and without ϕ angle correction.*

Source: Original

The polar angle was expected to increase with the tether length, making the airfoil maintain an approximately constant altitude. This expectation is based on results of off-line trajectory optimizations as the one shown in figure 3.2, however, the optimal operation altitude depends on several factors and there is no guarantee that a near constant altitude solution is the best solution for different wind profiles. More experimentation with different wind profiles will be required to further investigate the elevation angle variation.

It can also be observed that the optimal reeling speed has sudden variations. This happens because the optimization was not executed at every time step but at a slower frequency. Although the optimization routine runs relatively fast in MATLAB with a modern computer, finishing in approximately 200 ms, it is more realistic to assume a slower execution frequency in a real implementation, since the hardware limitations are

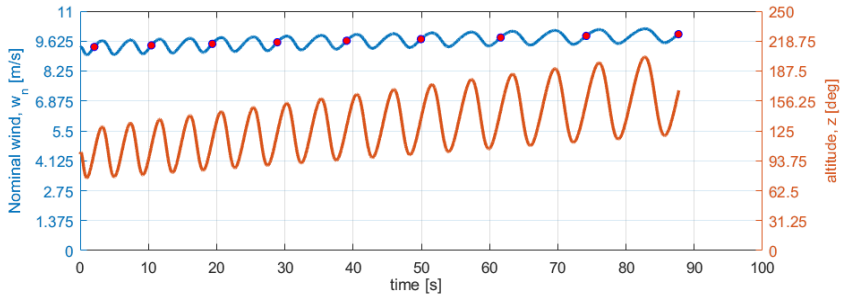

Figure 5.7: *Nominal wind speed at the airfoil's altitude (blue) and airfoil's altitude (orange) during the simulation. The red dots indicate the end of each lemniscate figure where the the airfoil is at* $\phi = 0$.

Source: Original

usually more strict in practice.

In a second scenario of simulation, the wind speed was increased and the power and tether traction constraints were reduced to 50kW and 3000N. The objective of this simulation is to observe how the optimizer would react to tougher conditions.

Figures 5.8 shows the resulting kite trajectory. The trajectory is shown from a lateral view to highlight the elevation angle variation. It can be seen that the trajectory goes, right at the start, to a smaller polar angle and gradually increases as the tether is reeled out.

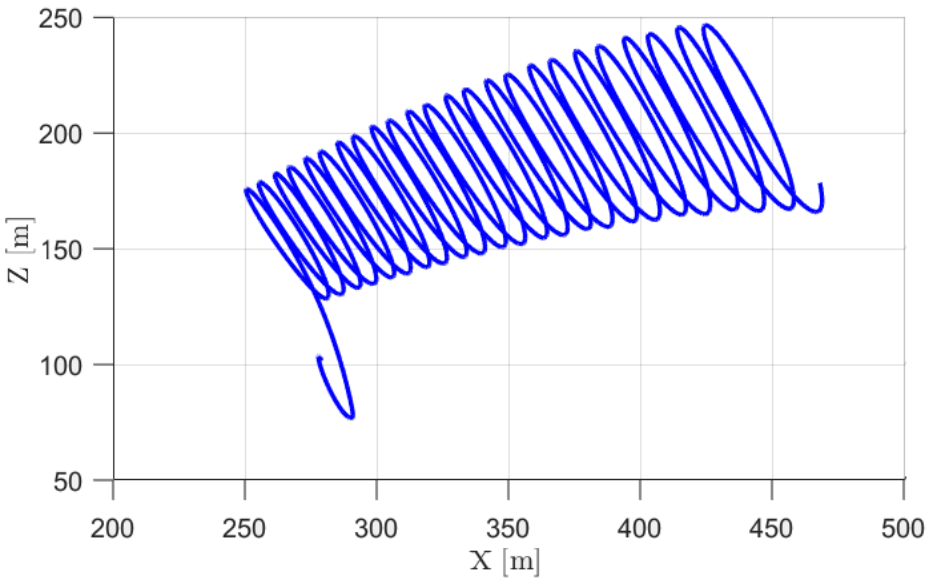

Figure 5.8: *Lateral view of the airfoil's trajectory during a simulation under high wind conditions and severe restrictions.*

Source: Original

The number of complete lemniscates also indicates that the reeling speed is much

smaller than the previous scenario. This is confirmed in figure 5.9, where it is clear that the reeling speed is kept at a low value during the whole trajectory. Both these differences are explained by observing the tether traction force and the electric machine's power in figure 5.10, where it is clear that both the tether traction force and the mechanical power are at the constraints' limits. The optimizer reduced the reeling speed to reduce the mechanical power, however, with a lower reeling speed the traction force is increased, requiring a smaller elevation angle to remain within the imposed constraints.

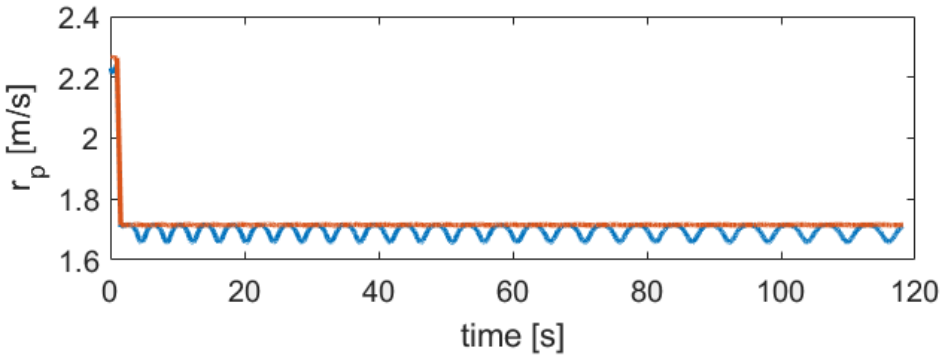

Figure 5.9: *Tether reeling speed with and without ϕ angle correction under high wind speeds.*

Source: Original

It is important to remember that the traction force and power values considered in the optimization are an approximation of the cycle power considering the airfoil in equilibrium at the central position of the lemniscate. Therefore the actual values considered by the optimization are the ones correspondent to the red dots in figure 5.10. The observed tether traction force and mechanical power values violate the constraints at other trajectory points. This must be considered when defining the restriction values.

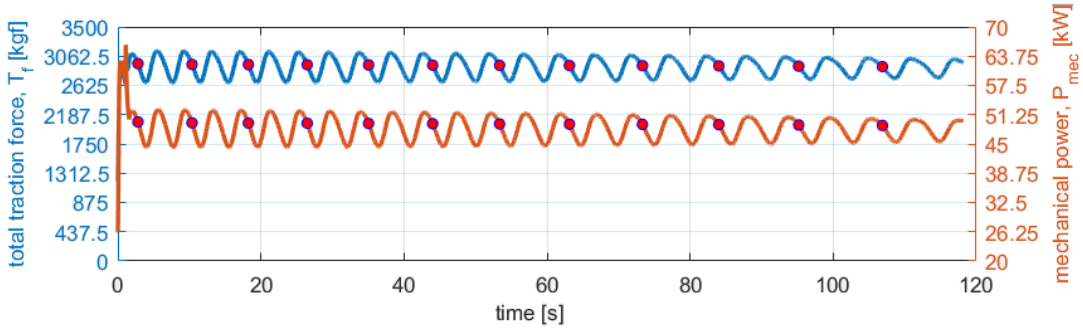

Figure 5.10: *Total tether traction force and machines mechanical power under high winds and severe restrictions. The red dots indicate the beginning of a lemniscate loop.*

Source: Original

Chapter 6

Final remarks

This work presented an on-line trajectory generation strategy for a pumping-kite energy generation system. The solution proposed was designed to achieve a near optimal cycle power while allowing it to adapt its operation to a large set of operation constraints. An economic NMPC was used to generate the retraction phase trajectory, and previously proposed optimization procedures for the traction phase were adapted into an online optimization. A simple criterion to operate during the transition phase was suggested, covering, in the end, all operating phases of a pumping-kite system. The solution proposed aimed to combine the best of the solutions found in the literature by allowing for multiple operational and physical constraints and the current wind condition to be taken into account in a decentralized control architecture.

The retraction phase strategy proposed showed promising results, obtaining a behavior close to the optimal off-line generated ramps from the literature but allowing for more complex reference curves than the previously used ramps, consequently better exploiting the system's capacities. A model mismatch treatment was applied to guarantee zero steady-state prediction error for the NMPC controller and avoid disrespecting constraints. The use of soft constraints enabled a more robust MPC execution, avoiding the construction of QP problems with no solution. The cost function employed allows for the use of very small prediction horizons resulting in a fast solution, while still obtaining a very good cycle power.

The proposed solution also does not directly optimize the cycle power. Although a brief study was conducted to propose a weight heuristic that improves this metric, the final solution proposed is fairly simple, and it is believed that a slightly more complex heuristic can further improve the results.

A traction phase optimization strategy borrowed from the literature was adapted to a real time optimization by approximating the cycle power in the cost function using values measured in the previous retraction and transition phases. It was also broken down into two different optimization procedures: an operation point optimization, and a tether speed and elevation angle optimization, each with different execution frequencies. The cost function simplification obtained very close results to the off-line optimization routines in which it was based. The on-line optimization of the reeling-speed and the elevation angle also achieved excellent constraint compliance, successfully adapting

the solution to a restrict set of constraints.

Inspired by the model mismatch treatment applied to the PNMPC, a similar treatment was proposed to ensure that the optimal reeling speed calculated would be applied through the traction control.

This work did not cover a simulation scenario where either the traction phase model mismatch treatment, or the operation point optimization could be tested. However, similar implementation of both algorithms were implemented and obtained good results, since the operation point optimization is almost identical to tether reeling speed and elevation angle optimization, and a model mismatch treatment was applied to the retraction phase. A full-cycle integrated simulation under the presence of disturbances will be conducted in future works to validate these two points and two provide a better approximation of the cycle power obtained with the complete solution. Only then a more fair comparison can be made with full cycle optimization works.

6.1 Future works

As previously mentioned, the most critical future work is to provide a full implementation of the trajectory optimization on-line algorithm and validate it under a full-cycle simulation under the presence of noise and wind gusts. This will enable a more thorough evaluation of the proposed solution and test the remaining modifications proposed.

Although good results were obtained in initial simulations, the proposed solution was also not tested in a real system. Therefore, after a complete version of the solution is validated in simulation, a natural next step for this work would be to implement an embedded version of the proposed algorithms in C, using a QP framework, and check if it is applicable in practice. For the purpose of a practical implementation many changes to the NMPC algorithm can be made to allow for a faster execution time, and better response. Here are some possible modifications:

- Instead of using the full aerodynamic surfaces in the NMPC model, approximate, at each NMPC iteration, the surfaces by polynomials or tangential planes, providing analytical expressions for the aerodynamic coefficients and, consequently, to the full model.

- Use an automatic differentiation tool and analytical expressions for the model dynamics to calculate the free responses and G_{PNMPC} matrices without requiring to simulate the system.

- Recalculate the G_{PNMPC} matrices only after a few sample periods, assuming that the previous linearization is still a reasonable approximation of the system.

Due to the simplicity of the employed model, a significant model mismatch is expected. In particular, a real system will present significant computational delays for the acquirement and processing of information and actuation dynamics. The depower actuation is further jeopardized as the references are calculated in the ground unit and must be sent to the airborne control pod. This adds on extra delay for the data transmission. This problem can be mitigated by measuring the mean actuation delay and including it in the NMPC model. This would require a bigger prediction horizon but can significantly improve the results.

Finally, to use a simpler economic NMPC to generate a retraction trajectory is a new approach of retraction phase optimization, being first explored in this work. Countless variations of MPC algorithms, cost functions and weight heuristics can be explored, potentially achieving better results.

For the traction phase optimization it is imperative to integrate the already implemented solution with the traction control system and the model mismatch treatment. A more intuitive and direct control architecture to deal with the wind gusts problem can be investigated as the reeling speed correction control loop may require a very slow dynamic to avoid interaction with the inner control loops. A further investigation of the tether reeling speed and elevation angle variations under different wind conditions must be carried to identify the most relevant effect that defines observed behavior and the discrepancy found by other trajectory optimization works.

Bibliography

[1] *Altaeros Energies*. http://www.altaerosenergies.com/, Accessed in July, 2017.

[2] *Enerkite brochure*. http://enerkite.de, Accessed in July, 2017.

[3] *Makani Power*. https://x.company/makani/, Accessed in July, 2017.

[4] US Energy Information Administration. Annual energy outlook 2016 levelized costs. Technical report, US Energy Information Administration (eia), Agosto 2016.

[5] International Energy Agency. Technology roadmap - wind energy, 2013.

[6] Cristina L. Archer and Mark Z. Jacobson. Evaluation of global wind power. *Journal of Geophysical Research*, 110, 2005.

[7] HHJ Bloemen, TJJ Van den Boom, and HB Verbruggen. Model-based predictive control for hammerstein systems. In *Decision and Control, 2000. Proceedings of the 39th IEEE Conference on*, volume 5, pages 4963–4968. IEEE, 2000.

[8] Hans Georg Bock and Karl-Josef Plitt. A multiple shooting algorithm for direct solution of optimal control problems. *IFAC Proceedings Volumes*, 17(2):1603–1608, 1984.

[9] Massimo Canale, Lorenzo Fagiano, and Mario Milanese. High altitude wind energy generation using controlled power kites. *IEEE Transactions on Control Systems Technology*, 18(2):279–293, 2010.

[10] Antonello Cherubini, Andrea Papini, Rocco Vertechy, and Marco Fontana. Airborne wind energy systems: A review of the technologies. *Renewable and Sustainable Energy Reviews*, 51:1461–1476, 2015.

[11] M. De Lellis, A.K. Mendonça, R. Saraiva, A. Trofino, and Á. Lezana. Electric power generation in wind farms with pumping kites: An economical analysis. *Renewable Energy*, 86(C):163–172, 2016.

[12] Marcelo De Lellis. *Airborne wind energy with tethered wings: modeling, analysis and control*. PhD thesis, Federal University of Santa Catarina, 2016.

[13] Moritz Diehl. *Real-time optimization for large scale nonlinear processes*. PhD thesis, 2001.

[14] Moritz Diehl. Airborne wind energy: Basic concepts and physical foundations. In *Airborne wind energy*, pages 3–22. Springer, 2013.

[15] Lorenzo Fagiano. *Control of tethered airfoils for high–altitude wind energy generation*. PhD thesis, Politecnico di Torino, 2009.

[16] Lorenzo Fagiano and Trevor Marks. Design of a small-scale prototype for research in airborne wind energy. *IEEE/ASME Transactions on Mechatronics*, 20(1):166–177, 2015.

[17] Jesus Garcia. Period optimal control and model predictive control of a tethered kite for airborne wind energy. Master's thesis, Delft University of Technology, July 2016.

[18] Martín Jorge Pomar García et al. Controle preditivo não linear com aplicação à eletrônica de potência. 2005.

[19] Peter Harrop. Awe: Electricity from kites and drones comes to market, 2017.

[20] Jannis Heilmann and Corey Houle. *Economics of Pumping Kite Generators*, pages 271–284. Springer Berlin Heidelberg, Berlin, Heidelberg, 2013.

[21] Greg Horn, Sébastien Gros, and Moritz Diehl. Numerical trajectory optimization for airborne wind energy systems described by high fidelity aircraft models. In *Airborne wind energy*, pages 205–218. Springer, 2013.

[22] Boris Houska and Moritz Diehl. Optimal control for power generating kites. In *Control Conference (ECC), 2007 European*, pages 3560–3567. IEEE, 2007.

[23] Marcos Jerez Venegas. Path optimization of a pumping kite system. Master's thesis, Delft University of Technology, July 2017.

[24] Miles L. Loyd. Crosswind kite power. *Journal of Energy*, 4:106–111, 1980.

[25] Agustinho Plucenio et al. *Desenvolvimento de técnicas de controle não linear para elevação de fluidos multifásicos*. PhD thesis, 2010.

[26] José Eli Santos Dos Santos et al. Controle preditivo não-linear para sistemas de hammerstein. 2007.

[27] Ramiro Saraiva. Aerofólios cabeados para geração de energia elétrica. Master's thesis, Universidade Federal de Santa Catarina, 2014.

[28] Ramiro Saraiva, Marcelo De Lellis, and Alexandre Trofino. Passive phase design of a pumping kite wind generator. *IFAC Proceedings Volumes*, 47(3):6764–6769, 2014.

[29] Eduardo Schmidt. A state estimation strategy for the monitorin, control, and optimization of airborne wind energy systems. Master's thesis, Federal University of Santa Catarina, 2017.

[30] UCS. A short history of energy, 2015. Acessed March 30, 2017.

[31] Rolf van der Vlugt, Johannes Peschel, and Roland Schmehl. Design and experimental characterization of a pumping kite power system. In *Airborne wind energy*, pages 403–425. Springer, 2013.

[32] Aldo U Zgraggen, Lorenzo Fagiano, and Manfred Morari. Real-time optimization and adaptation of the crosswind flight of tethered wings for airborne wind energy. *IEEE Transactions on Control Systems Technology*, 23(2):434–448, 2015.